공학박사 학위논문

Three Dimensional Assembly of Nanoparticles based on Electric-field Assisted Aerosol Lithography

전기장 보조 에어로졸 리소그래피를 이용한 3 차원 나노입자 조립

2016 년 2 월

서울대학교 대학원

기계항공공학부

최 호 섭

전기장 보조 에어로졸 리소그래피를 이용한 3 차원 나노입자 조립

Three Dimensional Assembly of Nanoparticles based on Electric-field Assisted Aerosol Lithography

지도교수 최 만 수

이 논문을 공학박사 학위논문으로 제출함

2015 년 11 월

서울대학교 대학원

기계항공공학부

최 호 섭

최호섭의 공학박사 학위논문을 인준함

2015 년 12 월

위 원 장 이 준 식 (인)

부위원장 최 만 수 (인)

위 원 전 누 리 (인)

위 원 고 승 환 (인)

위 원 김 형 철 (인)

Three Dimensional Assembly of Nanoparticles based on Electric-field Assisted Aerosol Lithography

Hoseop Choi

Department of Mechanical and Aerospace Engineering

The Graduate School

Seoul National University

Abstract

Nanoparticles has been considered as the fundamental building blocks in nanotechnology due to their excellent properties compared to bulk materials. In spite of great advances in fabricating functional nanoparticles having designed properties, there has been few researches for assembling them into desired shapes or placing at the exact location. Therefore, developing bottom-up based nanoparticle assembly technique is essential for practical use of nanoparticles.

The aim of this research is to develop a dynamic nanoparticle assembly technique which has nanoscale resolution and practicality. Ion Assisted Aerosol Lithography (IAAL) is aerosol based nanoparticle assembly technique which manipulate charged aerosol by controlling local electric field. In previously reported IAAL, the shape of nanoparticle structure was determined by the geometry of the pre patterned photoresist. In this article, we proposed the novel

nanoparticle assembly method by which we can fabricate any shape of nanoparticle structure. With the new method, charged nanoparticles are deposited not through the fixed PR pattern nor the stencil mask, but movable stencil to assemble nanoparticles to form the intended shape.

The fundamental understanding of the electrostatic lens effect is essential to extend the boundary of IAAL method. Parameters affecting the charged nanoparticle motion was identified and their effect to focusing effect is studied for establishing a standard process of nanoparticle assembly. 3 factors; the mask-substrate distance, the deposition voltage, the ion accumulation voltage; mainly affect the electrostatic lens effect. Not only these controllable process parameters, the Brownian diffusion also does great effect on the electrostatic lens effect. Various 3D nanoparticle structure was fabricated based on understating the electrostatic lens effect. The charge transport inside the nanoparticle structure was investigated, and new nanoparticle deposition model was proposed and we validate the model by the experiment and the nanoparticle trajectory simulation.

To enhance the controllability of electrostatic lens effect, we propose new electrified mask method by applying an electric potential directly to the metal coated mask surface. The potential difference between the mask and the substrate generates electrostatic lens effect which makes charged nanoparticles deposited at the center of the mask opening. The electrostatic lens effect can be easily and precisely controlled by adjusting the potential difference between the mask and the substrate. Particle trajectories were calculated by solving the Langevin equation, and the resulting particle deposition profile was compared with the experimental results. Using this approach, a multi-material

nanoparticle cluster array was fabricated by a sequential deposition of silver and copper nanoparticles after lateral translation of the mask

We have fabricate 3D nanoparticle structure by translating the mask in deposition process. Depending on the translation speed, nanoparticle deposition process was divided into 2 different modes; writing mode and 3D printing mode. By controlling the translation shape and speed, various shapes of nanoparticle structure were fabricated. We proposed new parameters called modified translation speed which could be used as the criteria for separating the 3D printing mode and writing mode.

Keywords: Nanoparticles; Ion Assisted Aerosol Lithography; Electrostatic lens effect; 3D printing; Electrified mask;

Student Number: 2009-20736

Contents

List of Tables

List of Figures

1. Introduction

1.1. Background of Research

There is a growing interest in the assembly of nanoparticles (NPs), as they exhibit tunable optical and electrical characteristics in their assembled structures (Peng et al., 2000; Warner & Hutchison, 2003; Kim et al., 2006; Cheng et al., 2008). These characteristics of NPs create opportunities to utilize them in areas such as photonics (Ergin et al., 2010; von Freymann et al., 2010; Zhang et al., 2011), gas sensing (Ponzoni et al., 2006; Kim et al., 2011), and Li batteries (Park et al., 2010; Guo et al., 2011). To this end, a lot of research has been carried out to develop methods for precise positioning and printing of NPs in desired shapes. NP assembly can be accomplished by utilizing various mechanisms, such as electrostatic forces (Kim et al., 2006; Kalsin et al., 2006; Jiang et al., 2009), magnetic forces (Wolf & Birringer, 2005; Demirors et al., 2013), capillary forces (Lin et al., 2003; Vyawahare et al., 2006; Kraus et al., 2007), and selective molecular bonding (Nykypanchuk et al., 2008). While most of these techniques are suited for colloidal NPs, aerosol-based printing methods have drawn much attention for their advantages such as high purity of the NPs and mild processing conditions (Krinke et al., 2001; Motl et al., 2013).

Ion assisted aerosol lithography (IAAL) is an aerosol-based assembly technique, which utilizes the distorted local electric field induced by accumulated ions on pre-patterned substrate to manipulate the trajectory of charged NPs as they get drawn to the substrate by electrostatic attraction (Kim et al., 2006; Lee et al., 2009; Lee et al., 2010; Woo et al., 2011; Ha et al., 2014). IAAL uses ions that have accumulated on the photoresist (PR) pattern surface to induce the electrostatic lens effect which causes charged NPs to converge toward the center of the PR opening and deposit on the substrate underneath.

To eliminate multiple PR patterning steps, a reusable non-conduction mask was fabricated from Si_3N_4 or epoxy to hold ions that induce the electrostatic lens effect (You et al., 2010). This mask can be used repeatedly since the NPs are selectively deposited onto the substrate, not on the mask, which eliminates the need to prepare a new mask for each operation. Not only two dimensional nanoparticle pattering, three dimensional structure with complex shape can be also fabricated by IAAL method.

For developing IAAL techniques into general lithography methodology, it is absolutely required to understand fundamental principles of electrostatic lens effect and precise controlling of focusing effect for precise and consistent fabrication of 3D nanostructure.

In this thesis, we study the basic principles of electrostatic lens effects. Then we present new nanoparticle assembly technique for controlling of electrostatic lens effect via the electrified mask. Based on these studies, we extend the 2D nanoparticle assembly method to dynamic fabrication of 3D nanoparticle structure.

1.1.1. Ion Assisted Aerosol Lithography for nanoparticle assembly

Ion Assisted Aerosol Lithography (IAAL) is aerosol based assembly technique which utilize distorted local electric field induced by accumulated ions on the pre-patterned Photoresist (PR) surface to manipulate the trajectory of charged aerosol nanoparticles. (Kim et al., 2006; Lee et al., 2009; Lee et al., 2010; You et al., 2010; Woo et al., 2011; Kim et al., 2011; Jung et al., 2014)

When ions are supplied to the substrate with applying the negative potential to the substrate, ions are accumulated onto the PR surface, not onto the exposed conductive Si surface. (Figure 1.1) This imbalance of ion distribution distorts the local equipotential lines near the PR opening from linear alignment parallel to the substrate to concaving toward the substrate. These distorted electric act like nanoscopic electrostatic lens near each PR opening, which maneuvers charged nanoparticles to converge to the center of PR opening and to be deposited onto the substrate. (Figure 1.2) Subsequent removal of PR layers finally produces a nanoparticle array having a feature size much smaller than the original PR patterns.

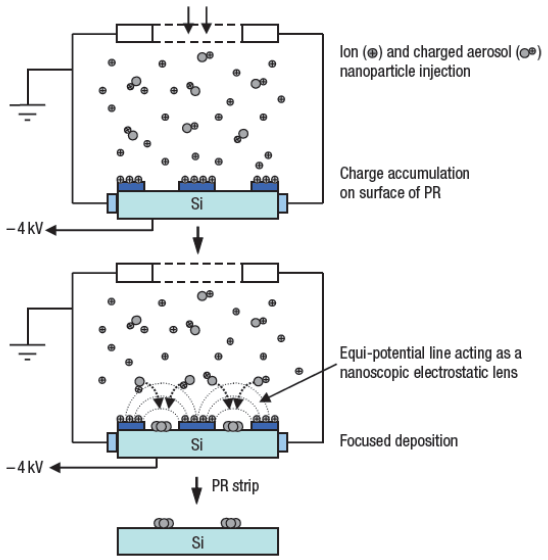

Figure 1.1. Schematics for electrostatic lens effect (adapted from H.Kim et al., 2009)

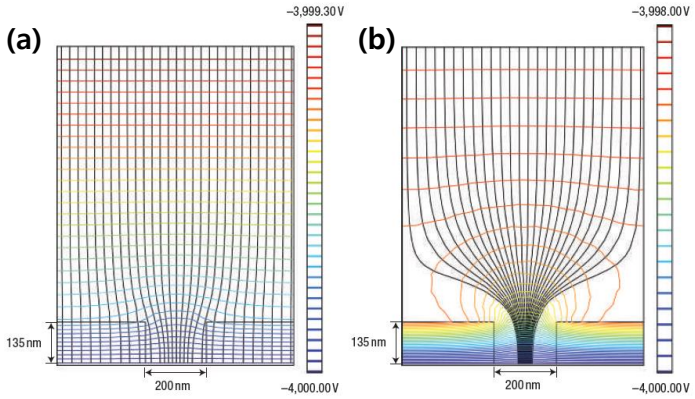

Figure 1.2. Equipotential lines and electric field line (a) without (b) with ion accumulations. (adapted from H.Kim et al., 2009)

1.1.2. Nanoparticle assembly via focusing mask

IAAL is a facile way for multiscale multidimensional assembly of nanoparticles. But before the particle deposition process, pre-patterning process is always need to fabricate nanoparticle array, which require the extra time and expense. To eliminate multiple PR patterning steps, a reusable non-conduction mask was fabricated from Si_3N_4 or epoxy to hold ions that induce the electrostatic lens effect. (You et al., 2010)

In this technique, pre-pattering process is now replaced by just placing the mask onto the substrate. Ion are accumulated onto the surface on the mask and induce the electrostatic lens effect. After nanoparticle deposition, fabrication process is finished by just detaching the mask from the substrate. This mask can be used repeatedly since the NPs are selectively deposited onto the substrate, not on the mask, which eliminates the need to prepare a new mask for each operation. (Figure 1.3)

Figure 1.4(a) shows line patterns consisting of silver particles on a Si substrate, obtained via the silicon nitride mask having 500nm openings. **Figure 1.4(b)** shows square pattern consisting of copper particles on a Si substrate, obtained via a silicon nitride mask having $4\times4\ \mu m^2$ square openings. Bottom images are silicon nitride masks used in experiments. This confirms an approximately 7 fold focusing capability of ion induced focusing mask approach.

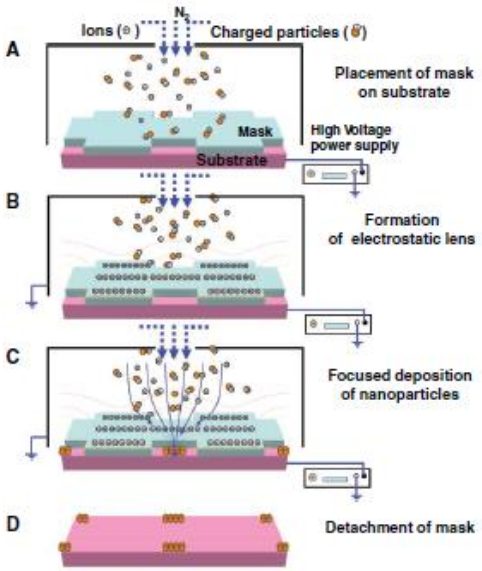

Figure 1.3. Experiment schematics of IAAL using ion induced focusing mask. (adapted from S.You et al., 2012)

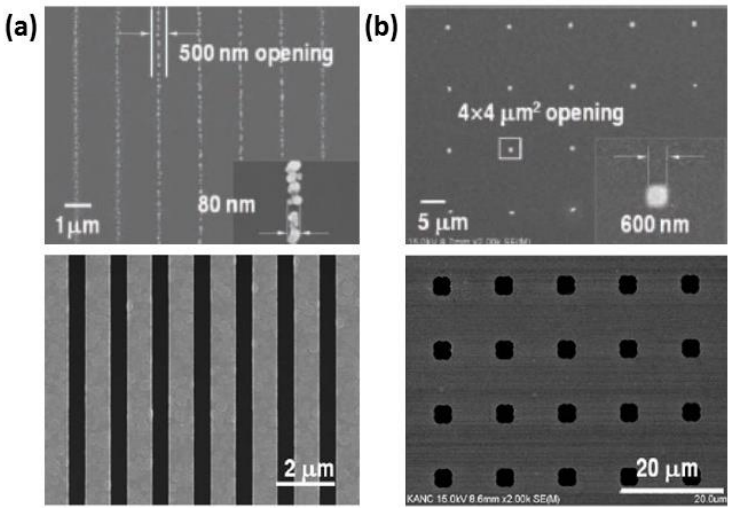

Figure 1.4. (upper) Nanoparticle arrays via ion induced mask (lower) ion induced mask used for nanoparticle assembly. (adapted from S.You et al., 2012)

1.2. Objective of Research

The main purpose of this research is to develop a dynamic nanoscale 3 dimensional nanoparticle printing technique based on Ion assisted aerosol lithography (IAAL) with reliability and practicality. As previously reported nanoparticle assembly techniques based on IAAL, charged aerosol nanoparticles (metal, oxide, protein, polymer, etc.) are mainly assembled in 2 dimensional array with a nanoscale resolution in parallel manner. The method for three dimensional assembly of aerosol nanoparticles is also reported. This method can fabricate complex shape of 3D nanoparticle structures which could not be attainable by conventional lithography methods, but their final product is determined by pre-patterned photoresist pattern shape. The goal of this research is develop a 3D nanoparticle printing technique of which final product is not restricted by pre-patterned PR shape, but is determined by the trajectory of the floating nanoparticle focusing mask which is translated in three dimensional.

Firstly, the fundamental understanding of the electrostatic lens effect is essential to extend the boundary of IAAL method. Parameters affecting the charged nanoparticle motion should be identified and their effect to focusing effect is studied for establishing a standard process of nanoparticle assembly.

Secondly, to improve the reliability and controllability of electrostatic lens effect, a novel technique for printing of charged nanoparticles using a metal coated stencil mask is demonstrated. By applying electric potentials to the mask and the substrate, electrostatic lens effect can be precisely engineered, which results controlled printing of charged nanoparticles.

Numerical simulation for particle trajectory is performed to validate the experiment data.

Lastly, dynamic three dimensional fabrication of nanoparticle structure would be proposed by translating the floating mask in three dimensional. Shape of nanoparticle structure could be determined in real time by actively translating the mask position. Various geometry of nanoparticle structure would be fabricated.

2. **Experimental Details**

2.1. Introduction

The basis of experimental setups is identical to previously reported IAAL methods. Spark discharge method was used for nanoparticle generation and generated charged nanoparticles were transported to ESP for nanoparticle deposition. In each experiments, they had almost same experiment configuration but little differences in the mask-substrate installation for satisfying the experiment objective. In this chapter, we explain experiment setups used commonly and analysis methods for interpretation of experiment results such as electric field simulation and nanoparticle trajectory simulations.

2.2. Spark discharge for generation of charged nanoparticles

Spark discharge method was used to generate NPs as it is a facile way to obtain charged NPs whose mean diameter and number concentration can be easily tuned by adjusting the process parameters such as discharge voltage and frequency, carrier gas flow rate, and electrode shape (Tabrizi et al., 2009; Han et al., 2012; Chae et al., 2014). When a voltage applied between the two metal electrode become higher than breakdown voltage, spark occurs between two electrodes and evaporate electrode materials near the spark point by heat and ion sputtering during spark discharge. The evaporated material is rapidly cooled down by carrier gas and condensed to nanoparticles. **Figure 2.1** illustrates the experimental set-up consisting of a spark discharge chamber, a deposition chamber, and a size distribution measurement system. For real-time measurements of the particle size distribution, a scanning mobility particle sizer

(SMPS) system, which is comprised of an aerosol neutralizer (TSI 3077), a differential mobility analyzer (TSI 3085), and a condensation particle counter (TSI 3776), was installed between the spark discharge chamber and the deposition chamber. In most experiments, the pin-to-plate type spark discharge method is used. For the pin-to-plate charge discharge method, since the nanoparticle are generated near the exit hole of the plate electrode, and transported immediately after generation, smaller nanoparticle are produced compared to the widely used rod-to-rod spark discharge method. Cu (99.99% purity) are used for materials of nanoparticles. Spark discharge generation circuit is made by parallel connected 20MΩ resister and 2nF capacitor. The gap between the pin electrode and the plate was fixed at 1mm, and the center of exit hole coincides with the pin electrode. With this setup, charged silver NPs with a geometric mean diameter of approximately 5.1 nm were generated with a nitrogen flow at 4 lpm. (Figure 2.2)

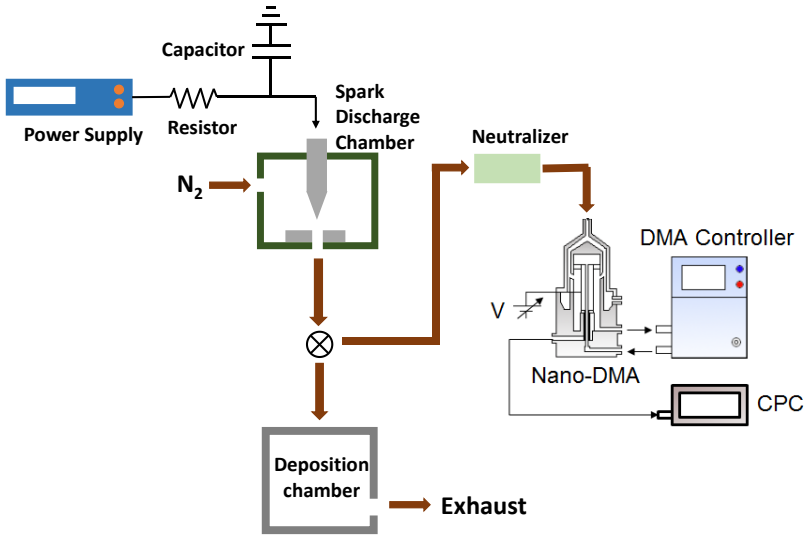

Figure 2.1. Experimental Setup consisting of a spark discharge chamber, a deposition chamber and a size measurement system (SMPS). (adapted from H.Choi et al., 2015)

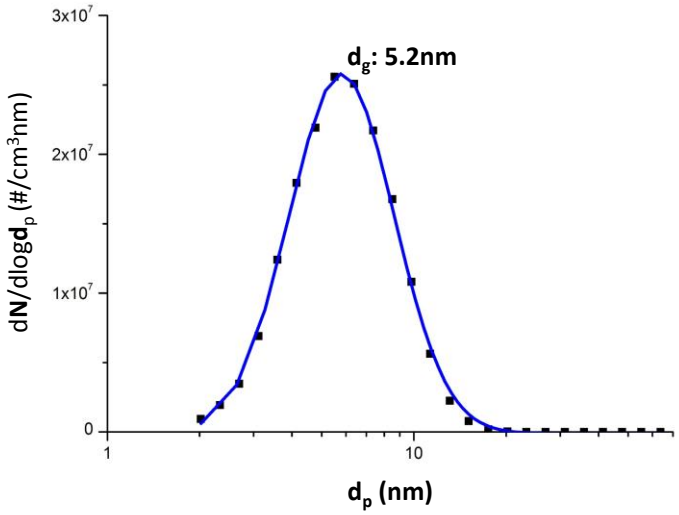

Figure 2.2. Distribution of generated Cu nanoparticles

2.3. Fabrication of a floating mask

The fabrication step of a floating mask is basically identical to Ion-induced focusing mask. The different point is that now the mask is placed above the substrate in fixed distance during the nanoparticle deposition process. Silicon nitride stencil mask is used in this experiment. Fabrication procedure is explained in **Figure 2.3**. The 1 μm thick Si_3N_4 stencil mask was fabricated by coating a Si wafer with 1 μm thick low stress Si_3N_4 film and pattering it using photolithography and eliminating bottom Si layer via reactive ion etching process. Opening patterns of the mask consist of 4 μm wide line and 4 μm × 4 μm square patterns with 12 μm pitch. There are some process steps required attention. Many problems could occur in deep-etch for silicon nitride film. The most problem frequently occurring is under etching of silicon nitride film. Low stress Si_3N_4 film has high chemical resistance, so PR layer could not endure whole etch process, which leads the under-etching problem.

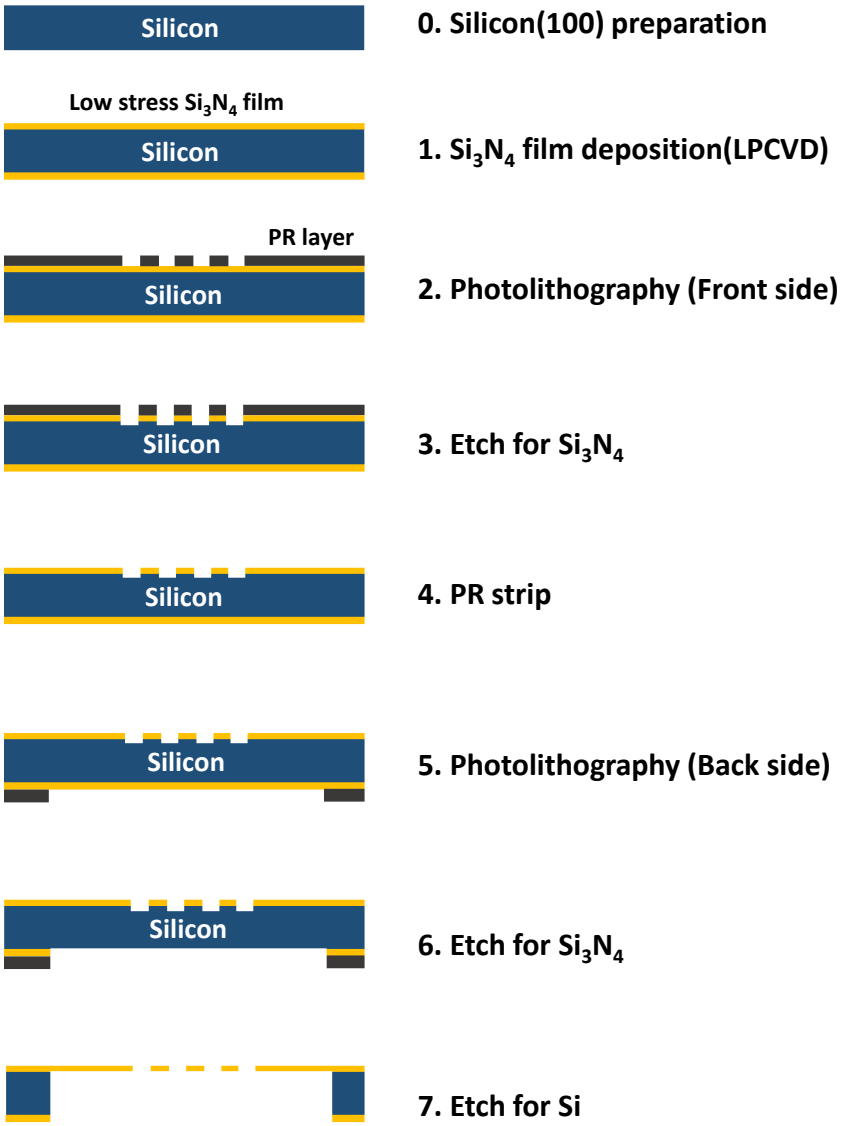

Figure 2.3. Fabrication procedure for Si_3N_4 nitride stencil mask

2.4. Experimental Procedure

The experimental procedure is illustrated in **Figure 2.4**. It is noted that now the mask is placed above the substrate with fixed distance, and the effect of the gap between the mask and substrate to electrostatic lens effect was examined in this experiment. The distance between the mask and the substrate was determined by thickness of PR which is coated onto the substrate, and the nanoparticle deposition area was etched so the PR is only acted as a spacer. 3 types of the substrate were prepared; Bare Si, Si wafer coated with 4 μm thick PR and 8 μm thick PR. The substrate was attached onto the electrode with carbon tape, and the nanoparticle focusing mask was placed on the substrate. The mask and the substrate were tied up by the ceramic holder. The installation of the substrate and the mask is depicted in **Figure 2.5.** After placing the mask above the substrate, ions were supplied to the deposition chamber. Ions were generated by corona discharge method with nitrogen flow at 3 lpm, and corona discharge chamber was pin-to-plate type. Amount of ion accumulation on the mask surface is controlled by an ion deposition voltage which is applied to the substrate during the ion accumulation process, so it is import to generate same ion flow for each experiment. Amount of ions generated corona discharge was measured by Faraday-cup electrometer and average current value was 7.5 pA. Applied voltage to the corona discharge chamber was ranged from 3.0 – 4.0 kV. Charged nanoparticles were injected to the deposition chamber after ion accumulation process. No ions were supplied during the nanoparticle deposition process. Nanoparticle deposition time was changed depending on the nanoparticle generation rate. Size distribution of generated nanoparticles was measured for each experiments, and deposition time was determined by

total nanoparticle concentration for insuring the same amount of charged nanoparticles was supplied for each operation. The reference total concentration and deposition time was 2.0×10^7 #/cm^3 and 40 minutes. After deposition process, the result structure was observed by Scanning Electron Microscopy (SEM) and the width of nanoparticle structure was measured.

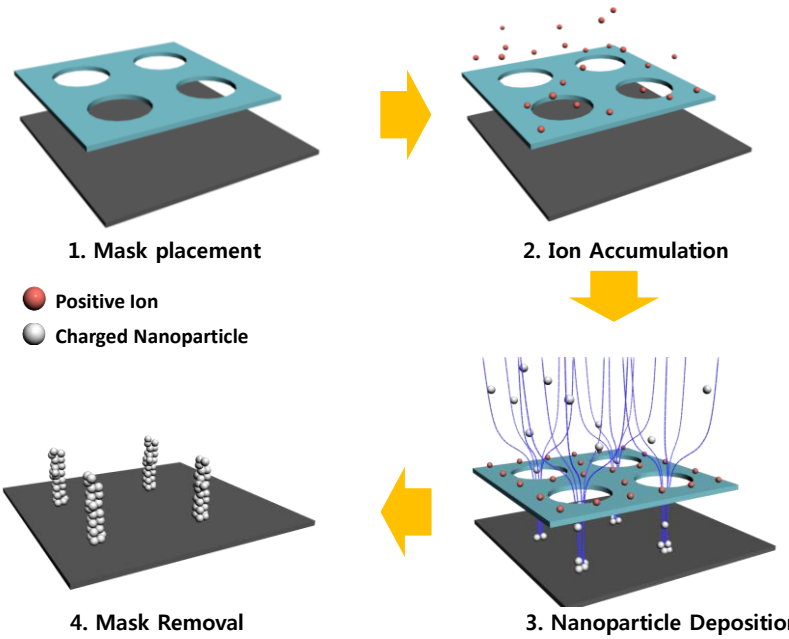

Figure 2.4. Experimental procedure of IAAL via a floating mask

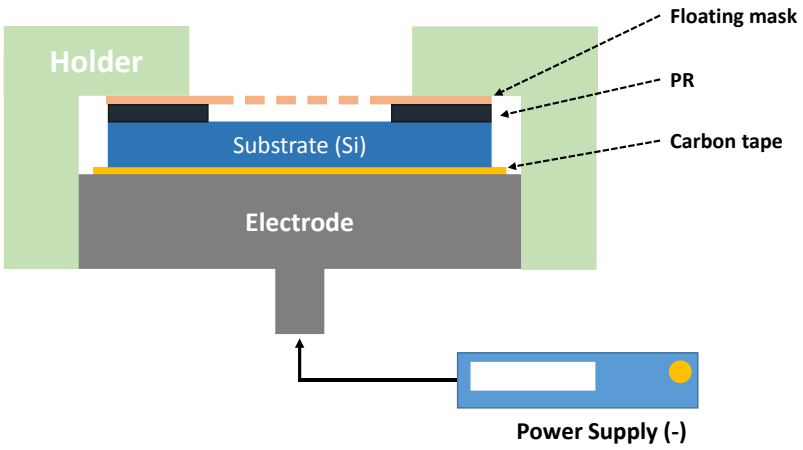

Figure 2.5. Setup for the mask and the substrate

2.5. Electric field and particle trajectory simulations

To investigate the mechanism of electrostatic focusing of charged NPs, the electric field calculations were carried out using electrostatic modules of COMSOL multiphysics 4.3.

The trajectories of the charged particles were calculated by solving the Langevin equation taking into account drag force (F_D), Brownian diffusion force (F_B), Coulomb force (F_C), and van der Waal's force (F_{vdW}) (You & Choi, 2007).

$$m_p \frac{dv_p}{dt} = F_D + F_B + F_C + F_{vdW}$$

Each of the force terms can be calculated by the following expressions.

$$F_D = f\left(v_g - v_p\right)$$

where f is the friction coefficient ($\mathrm{f} = 3\pi\mu\mathrm{d_p}/\mathrm{C_c}$, $\mathrm{C_c} = 1 + \lambda/\mathrm{d_p}\left[2.34 + 1.05\exp\left(-0.39\mathrm{d_p}/\lambda\right)\right]$) (Hinds, 1999) and v_g and v_p are gas and particle velocities, respectively (in this study, $v_g = 0$).

$$F_B = \sqrt{\frac{2k_B T f}{\Delta t}}\zeta$$

where k_B is the Boltzmann constant, T is the temperature and ζ is a zero-mean, unit-variance Gaussian random number (Li & Ahmadi, 1992).

$$F_C = qE$$

And

$$F_{vdW} = \frac{A_{H_{pgp}} d_p^3}{12\left(D_{C-S} - \frac{d_p}{2}\right)^2 \left(D_{C-S} + \frac{d_p}{2}\right)^2}\boldsymbol{n} + \frac{A_{H_{pgp}} d_p^6}{6\left(D_{C-C} - d_p\right)^2 D_{C-C}^3 \left(D_{C-C} + d_p\right)^2}\boldsymbol{r}$$

where A_H is the Hamaker constant (Visser, 1972).

3. Ion assisted aerosol lithography via a floating mask

3.1. Introduction

Ion assisted aerosol lithography (IAAL) is an aerosol-based assembly technique, which utilizes the distorted local electric field induced by accumulated ions on pre-patterned substrate to manipulate the trajectory of charged NPs as they get drawn to the substrate by electrostatic attraction (Kim et al., 2006; Lee et al., 2009; Lee et al., 2010; Woo et al., 2011; Ha et al., 2014). IAAL uses ions that have accumulated on the photoresist (PR) pattern surface to induce the electrostatic lens effect which causes charged NPs to converge toward the center of the PR opening and deposit on the substrate underneath. To eliminate multiple PR patterning steps, a reusable non-conduction mask was fabricated from Si_3N_4 or epoxy to hold ions that induce the electrostatic lens effect (You et al., 2010). This mask can be used repeatedly since the NPs are selectively deposited onto the substrate, not on the mask, which eliminates the need to prepare a new mask for each operation. Not only two dimensional nanoparticle pattering, three dimensional structure with complex shape can be also fabricated by IAAL method.

For developing IAAL techniques into general lithography methodology which is wieldy used, it is absolutely required to understand fundamental principles of electrostatic lens effect, which leads to precise controlling of focusing effect.

In this chapter, we study the basic principles of electrostatic lens effects. We examine parameters affecting electrostatic lens effects and mechanisms how they influence the focusing effect is studied.

3.2. Fabrication of nanoparticle cluster

Figure 3.1 shows SEM images for Cu nanoparticle cluster fabricated by a floating mask. Opening width of the mask was 4 μm and the gap between the mask and the substrate was set to be 8 μm. Positive N_2 ions were supplied in 20 mins, then Cu nanoparticles in 40 mins. The left image is line-patterned Cu nanoparticles with the width of 1 μm which is reduced by 4 times compared to the mask opening. The right image is square array of Cu nanoparticles cluster and square dot represents the mask opening. Even though the distance between the mask and the substrate is 8 μm which is longer 2 times than the mask opening, nanoparticles are deposited convergently toward the center region of the mask. No blurring effect can be found with even large gap between the mask and the substrate.

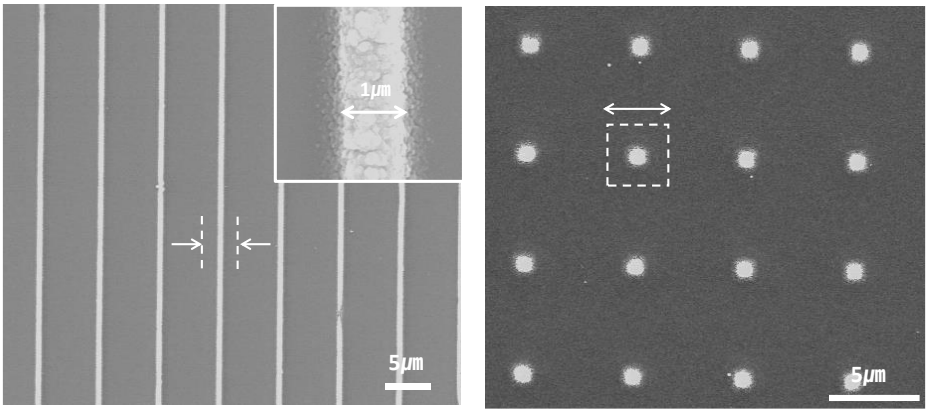

Figure 3.1. Patterned Cu nanoparticle fabricated by a floating mask

3.3. Parameters affecting the electrostatic lens effect

Figure 3.2 shows that changes in the width of nanoparticle cluster depending on three parameters. We controlled surface charge density on the mask surface, the distance between the mask and the substrate (d) and the deposition voltage (V_d) applied to the substrate. Surface charge density was regulated by the potential applied during the ion accumulation process (V_i; ion accumulation voltage). **Figure 3.3** shows the simulation result of ion accumulation process. Early stage of ion accumulation, the shape of electric field is parallel to mask surface. So ions were moving straight toward to the mask and the substrate, then deposited onto the mask surface. (Figure 3.3(a)) Accumulated ions distorted the local electric field near the mask opening into the concave shape. (Figure 3.3(b), (c)) As more ions were accumulated, less ions were approaching to the mask surface. Consequently, surface charge density reached some saturation point. (Figure 3.3(d)) This saturation point is determined by ion accumulation voltage(V_i) and the mask-substrate distance(d). Besides these parameters, experimental condition such as the size distribution of charged nanoparticles, temperature, humidity, and deposition time was controlled identically for each operation.

The most noticeable feature from the result is that the cluster width decreases with increasing the ion accumulation voltage. **Table 1** is the simulation result for saturation points of the surface charge density for each experimental condition. For each mask-substrate distance, the saturation point is proportional to V_i. It means more ions could be accumulated on the mask surface in case of enough supply of positive ions. Our experiment condition

satisfied this condition so the electrostatic lens effect gets stronger with increasing V_i. (**Figure 3.5**)

Generally, the pattern width deceases with increasing the mask-substrate distance in same condition in V_i and V_d. The electrostatic lens effect gets stronger with the distance between the mask and the substrate increasing. (**Figure 3.4**)

It is noted that the shape of the graph has U-shape which has minima at certain V_d. This is interesting result since it is known that the electrostatic lens effect gest stronger with decreasing V_d, which means pattern width would be linearly increased as V_d gets increased. **Figure 3.6** shows electric field simulations near the mask opening depending on V_d with constant surface charge density (9.5e-7 C/m^2). The distortion of the equipotential lines increases with decreasing V_d, causing the electric field lines to become more focused. Therefore, the expected pattern width acquired from the electric field simulation is proportionally increasing with V_d. But actual pattern width from the experiment shows opposite tendency in low V_d region. (**Figure 3.7**)

This discrepancy can be explained by considering Brownian diffusion. This fabrication method is processed in atmospheric conditions. If charged nanoparticle were just following the electric field, the shape of electric field could solely determine the electrostatic lens effects. But in real deposition process, Brownian diffusion exerts great influence on particle trajectory.

The uncertainty **Δr** acquired due to Brownian can be calculated by root-mean-square displacement.

$$\Delta r = \sqrt{2\Delta t D}$$

where Δt is time for a particle to deposit and D is Stoke-Einstein diffusion coefficient for nanoparticles, given by

$$D = \frac{C_c kT}{3\pi d\mu}$$

where C_c is Cunningham correction factor (Hinds, 1999), k is the Boltzmann constant, d is diameter of nanoparticle, and μ is viscosity of gas.

To simplify the calculation, nanoparticles would be assumed for moving at terminal velocity $\mathbf{v_t}$ balanced between the drag force and electrostatic force, which is given by

$$v_t = \frac{C_c q E_l}{3\pi d\mu}$$

where q is elementary charge, and E_l is local electric field density near the mask opening. Then we have the uncertainty due to Brownian motion Δr given by

$$\Delta r = \sqrt{r\frac{2kT}{qE_l}}$$

where r is the total translation distance of the nanoparticle.

It is noted that the uncertainty is inverse proportional to the strength of local electric field near the mask opening which is determined by the potential applied to the substrate.

The calculated value of the uncertainty due to Brownian motion is plotted in **Figure 3.8**, showing that the uncertainty decreases with increasing the deposition voltage.

The inconsistency between the experiment and the simulation in low V_d region can be explained by this uncertainty. In high V_d region (inertia dominant region), electric field strength near the mask opening is high enough to ignore the uncertainty due to Brownian motion. As a result, the trajectory of charged nanoparticles is manly determined by electrostatic force, and the width of nanoparticle cluster is determined only by the electrostatic lens effect. However, in low V_d region (diffusion dominant region), electric field strength is weak, so now Brownian motion has huge effect on the particle trajectory, the uncertainty is even bigger than expected pattern width from the electric field simulation. So in low V_d region, suppressing Brownian motion by increasing V_d leads to decreasing the width of nanoparticle cluster. The modified expected pattern width could be acquired by considering both the electrostatic lens effect and Brownian Diffusion, which is plotted in **Figure 3.9**.

This Brownian uncertainty can be expressed by dimensionless form after some modifications. The uncertainty **Δr** acquired due to Brownian is given by

$$\Delta \mathrm{r} = \sqrt{r\frac{2kT}{qE_l}}$$

And we put Stoke-Einstein diffusion coefficient D and terminal velocity $\mathbf{v_t}$ into the above equation**,** then we have

$$\frac{\Delta r}{r} = \sqrt{\frac{2h}{r^2}\frac{D}{v_t}} = \sqrt{\frac{2h}{r}\frac{D}{rv_t}}$$

The Peclet number is the dimensionless number which represents the ratio between advective transport rate and diffusive transport rate is given by

$$\mathrm{Pe} = \frac{Advevtive\ \ transport\ \ rate}{Diffusive\ \ transport\ \ rate} = \frac{rv_t}{D}$$

Then, we have dimensionless Brownian uncertainty which is given by

$$\frac{\Delta r}{r} = \frac{1}{\sqrt{Pe}}\sqrt{\frac{2h}{r}}$$

The graph of above equation is plotted in **Figure 3.10**

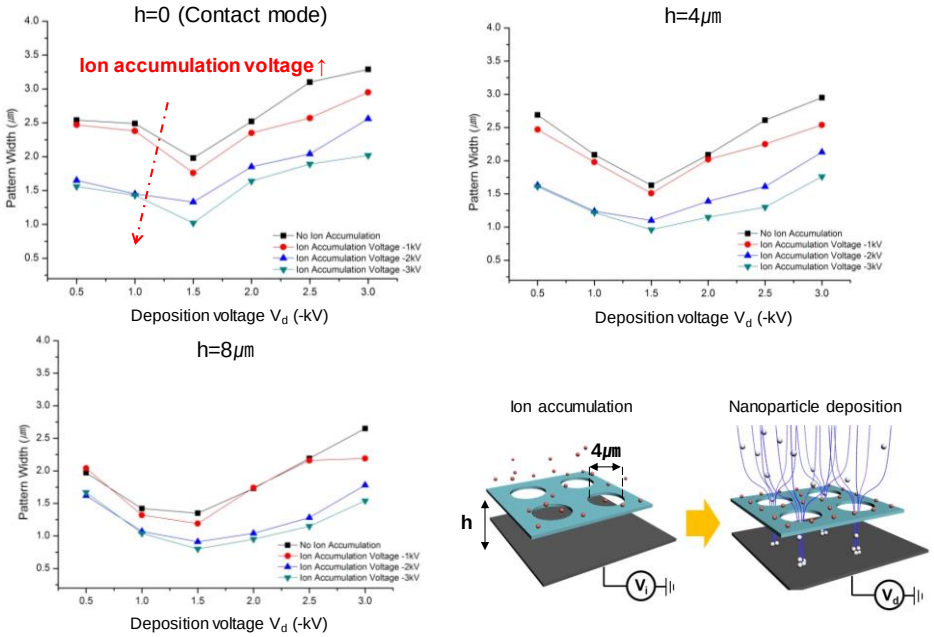

Figure 3.2. Changes in the patter width depending on parameters; mask substrate distance (d), ion accumulation voltage (V_i) and nanoparticle deposition voltage (V_d)

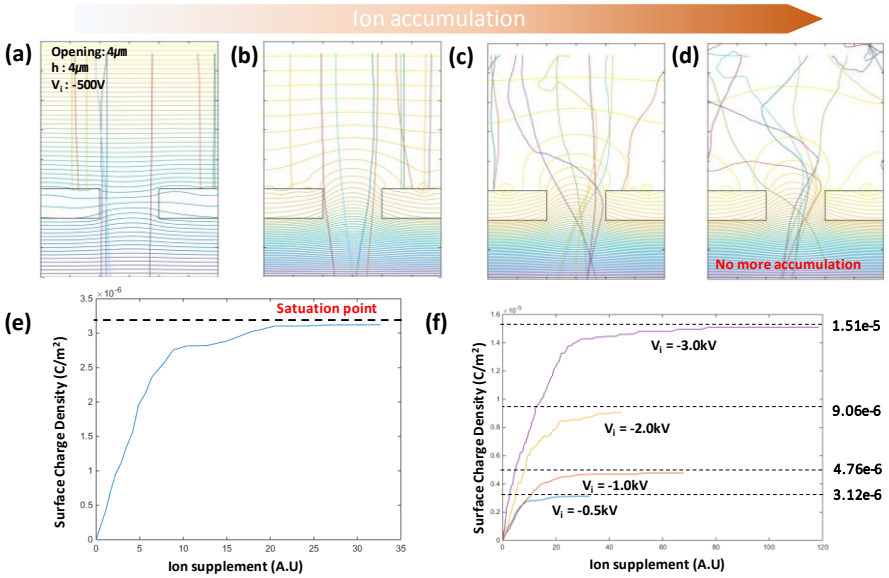

Figure 3.3. The result of ion trajectory simulation. (a)~(d) process of electrostatic lens formation (e) surface charge density on the mask surface (f) Saturation points depending on V_i

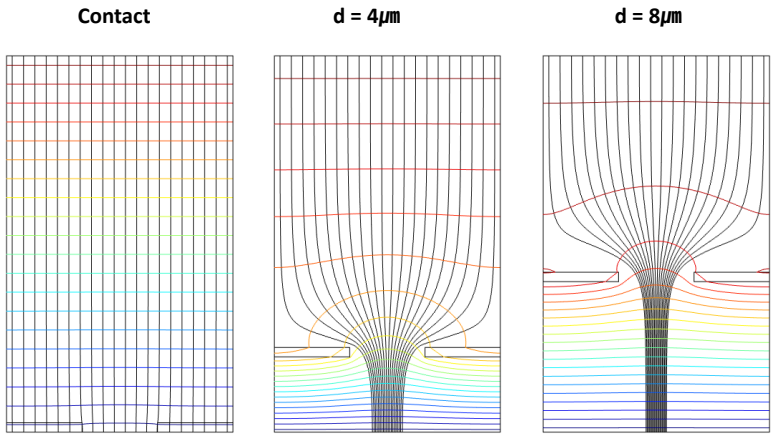

Figure 3.4. Electric field simulations with different distances between the mask and the substrate

		Ion Accumulation Voltage (V_i)			
		0.5kV	1kV	2kV	3kV
Distance (d)	Contact	7.14e-6	1.44e-5	2.87e-5	4.32e-5
	4 μm	4.62e-7	9.42e-7	1.86e-6	2.75e-6
	8 μm	2.96e-7	5.92e-7	1.18e-6	1.77e-6

Table 1. Saturation points of the surface charge density. [C/m^2]

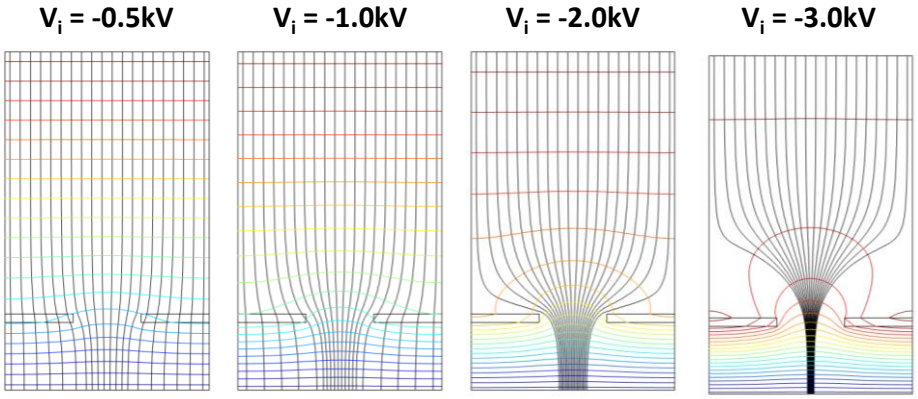

Figure 3.5. The electric field simulation results depending on V_i. V_d was constant for -2kV for each simulation

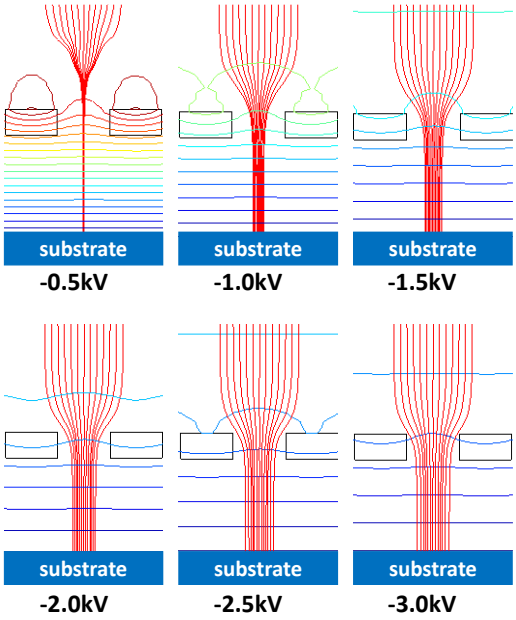

Figure 3.6. Electric field simulation result depending on the Vd. Surface charge density was constant for each simulation (σ_s = 9.5e-7 C/m^2)

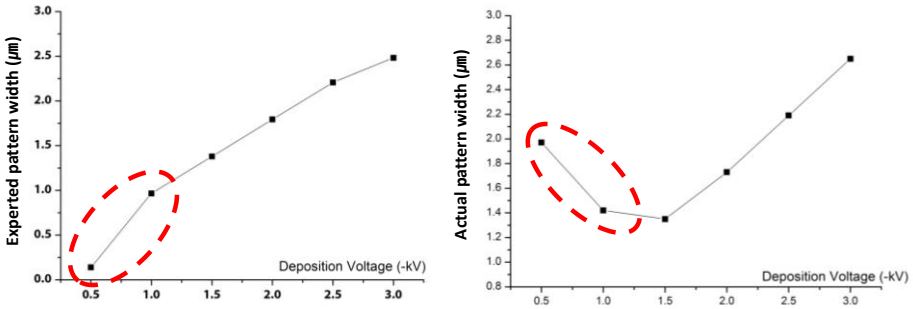

Figure 3.7. Expected and actual pattern width. (d = 4 ㎛, V_i = 1kV)

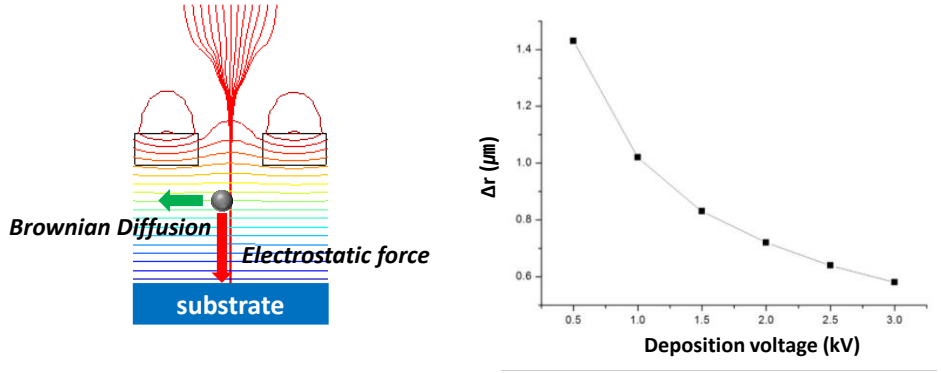

Figure 3.8. The uncertainty due to Brownian motion. The uncertainty decreases with increasing deposition voltage. The translation distance r was set to be the mask-substrate distance

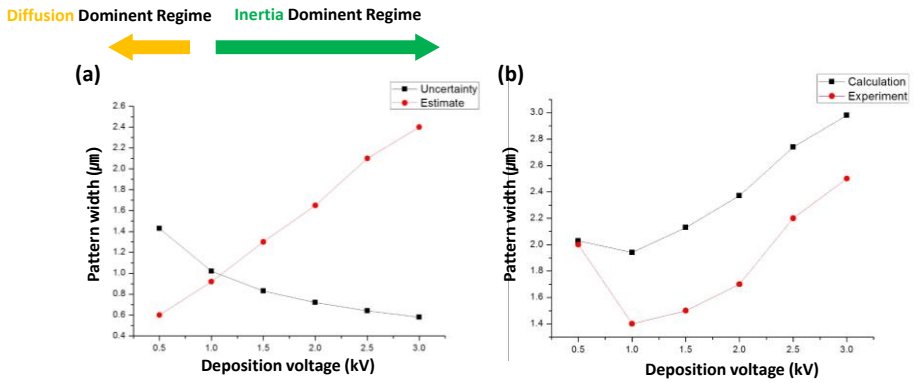

Figure 3.9. (a) The pattern width calculated by electric field simulation (red) and the uncertainty due to Brownian motion (black). (b) The modified expected pattern width considering Brownian motion (black) and actual pattern width from the experiment result. (red)

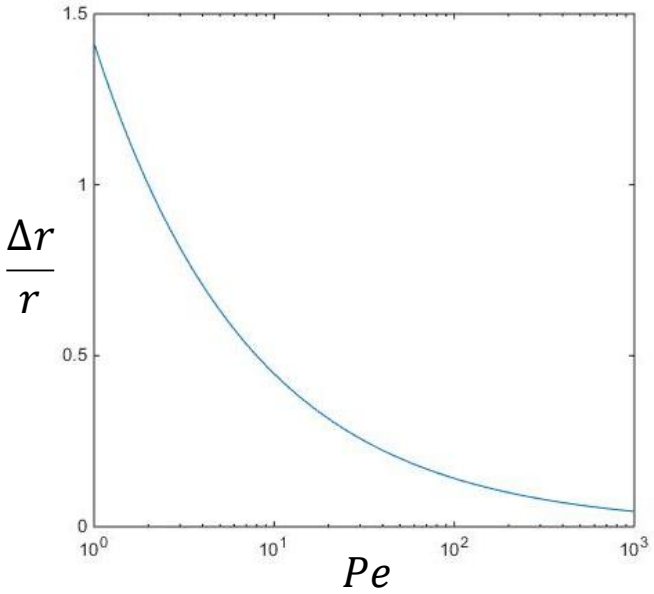

Figure 3.10. The dimensionless uncertainty by the Brownian diffusion

3.4. Nanoparticle material effect on pattern width

Properties of material consisting of nanoparticle itself does not affect the electrostatic effect. The Brownian uncertainty is only affected by the temperature and the electric field intensity. But the density of the material has influence on dynamics of nanoparticle motion.

The Stokes number is a dimensionless number characterizing the behavior of aerosol. The Stokes number is defined as the ratio of the particle relaxation time to the transit time past an obstacle.

$$\mathrm{Stk} = \frac{\tau_p}{\tau_f} = \frac{\rho_p C_c^2 d_p q E}{27\pi\mu^2 D_j}$$

where ρ_p is the density of the particle and D_j is the opening size of the pattern. When Stk>>1, particle continue moving in a straight line when the stream line bends; when Stk<<1, particle follow the streamlines perfectly.

Figure 3.11 shows the nanoparticle trajectory simulation for Cu and Au nanoparticles. Boundary conditions such as deposition voltage and surface charge density are same while density of the particles are different. With the same electrostatic focusing effect, particle trajectories are different because of particle's density. Because of small stokes number of copper nanoparticles, Cu nanoparticle structure has much smaller width compared to the gold nanostructure. **Figure 3.12** shows final particle deposition locations depending on materials. Copper has smaller density compared to gold, so the Stokes number is small. Charged copper particles can follow the electric field

streamline accurately. But the gold nanoparticle has big density so the stokes number is relatively big. So their inertia was large to follow the curved stream line. So actual trajectory of nanoparticles deviated from the electric field stream line, consequently pattern width is large compared to the copper case.

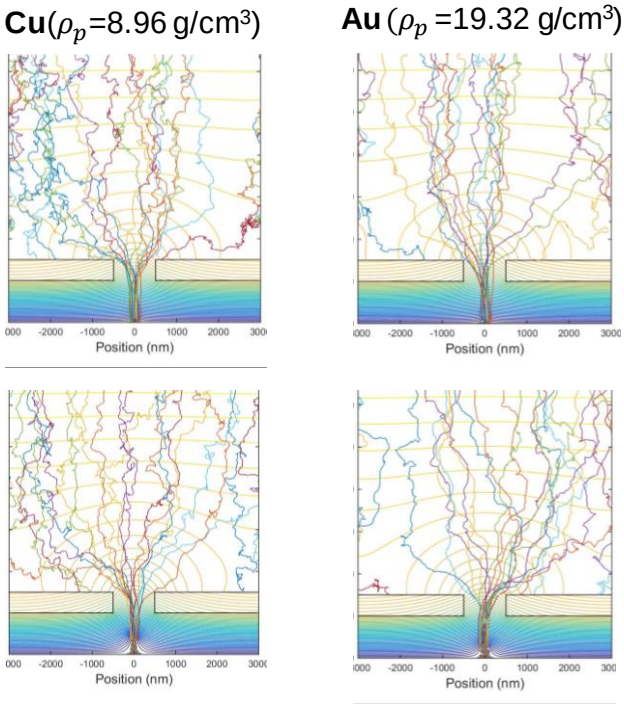

Figure 3.11 Nanoparticle trajectory simulation for Cu and Au nanoparticles

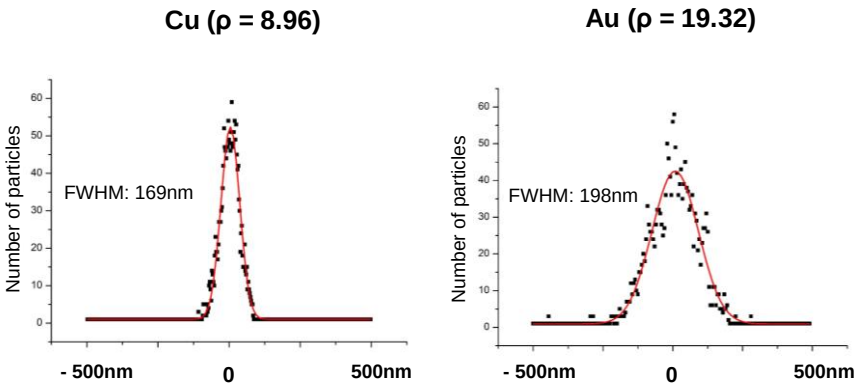

Figure 3.12 Histograms for final particle deposition locations depending on materials

3.5. Fabrication of 3D nanoparticle structure via a floating mask

Based on the study of the electrostatic lens effect, various shapes of 3D nanoparticle structures were fabricated via the floating mask method. The big advantage of the space between the mask and the substrate is that any kinds of substrate could be used for substrate. Figure 3.9 shows PSL nanoparticles deposited onto paper structure. PSL nanoparticles were atomized by the electrospray method, and the substrate was office paper. The mask was fabricated from the epoxy and the opening width was 50μm. **Figure 3.13** shows Cu nanoparticle clusters deposited in minima of the graph. (**d**=8 ㎛, $\mathbf{V_i}$ = -3kV, $\mathbf{V_d}$ = -1.5kV) In 20 mins deposition time, the shape of nanoparticle clusters was small bump. As the deposited structure was consisted of metal nanoparticles, the potential applied to the substrate was also applied to the structure itself. The electric field is concentrated at the sharp tip of the structure, so the trajectory of charged nanoparticles was toward to the top of the structure. With increasing the deposition time in 60 mins, nanoparticle was continuously deposited onto the top of the structures, then nanowires consisting of nanoparticles were fabricated. **Figure 3.14** shows nanowire array with deposition time of 120 mins. The mechanism of the fabrication of 3D nanoparticle structures was investigated by nanoparticle trajectory simulation. Since pre-deposited structures was consisting of metal nanoparticles, same voltage applied to the substrate was also applied to the nanoparticle cluster. Consequently, electric field intensity was enhanced at the top of the structures, then charged nanoparticle were attracted to the top of the structure, and

deposited. (**Figure 3.16 (c)**). We can observe storing electric field intensity at the top of the structures in **Figure 3.16 (d)**.

By changing $\mathbf{V_d}$ during the nanoparticle deposition process, interesting shapes of 3D nanoparticle structure could be fabricated. Our original plan was to fabricate nanowires having changing diameters in single nanowires. First, nanoparticles were deposited in 30min at $\mathbf{V_d}$ = -1.5kV, then deposited in 30min at $\mathbf{V_d}$ = -3.0kV in 30min. The result was core-shell structure. The core part was assumed to be deposited in 1st deposition process, and the shell part was formed in 2nd deposition process. This is an interesting result, as we expected that nanoparticles were deposited widely onto the top of the structures, and nanoparticle trajectory simulation also showed the same result as our expectation. (**Figure 3.18**) This phenomenon will be examined deeply in next chapter.

Various shapes of core-shell structures could be fabricated in different V_d. **Figure 3.19** shows various shapes of core-shell structures fabricated by changing V_d during the nanoparticle deposition process. Size of the core, shell, and the width of the core-shell distance was changed by controlling the deposition voltage and deposition times.

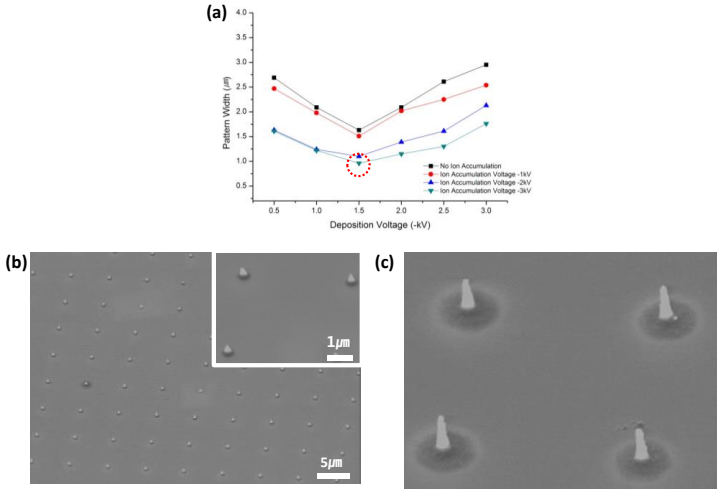

Figure 3.13. 3D nanoparticle assembly via the floating mask. (a) The experiment condition. The mask-substrate distance was 8 μm, and V_i and V_d is marked in the plot. (b) Nanoparticle clusters deposited in 20min (c) Nanoparticle cluster deposited in 60 mins.

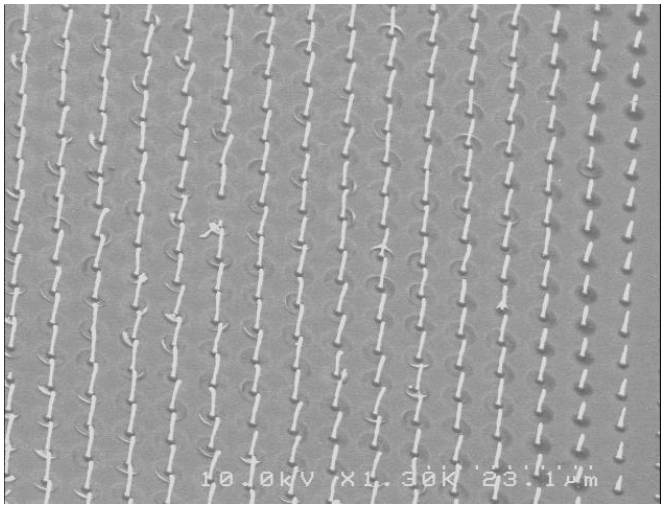

Figure 3.14. Nanowires consisting of Cu nanoparticles. Deposition time was 120 mins.

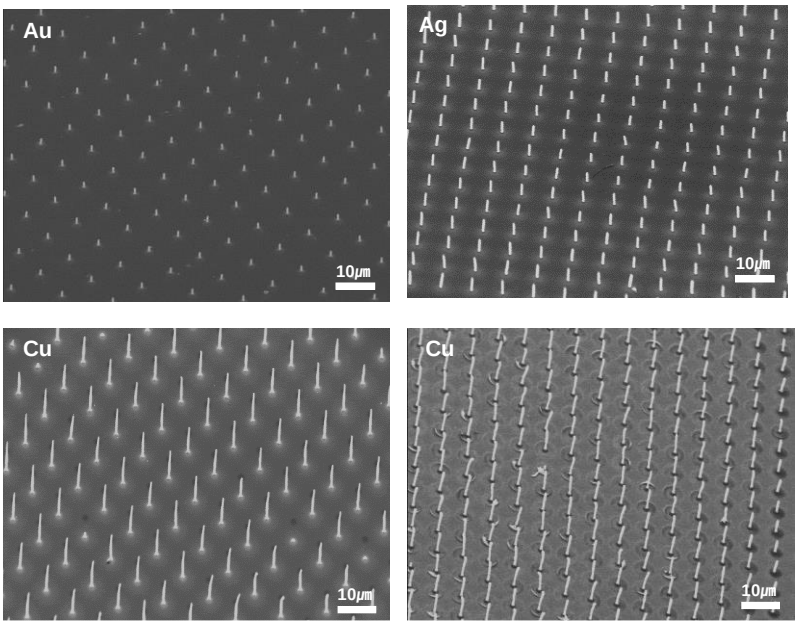

Figure 3.15. Nanowire arrays consisting of various materials

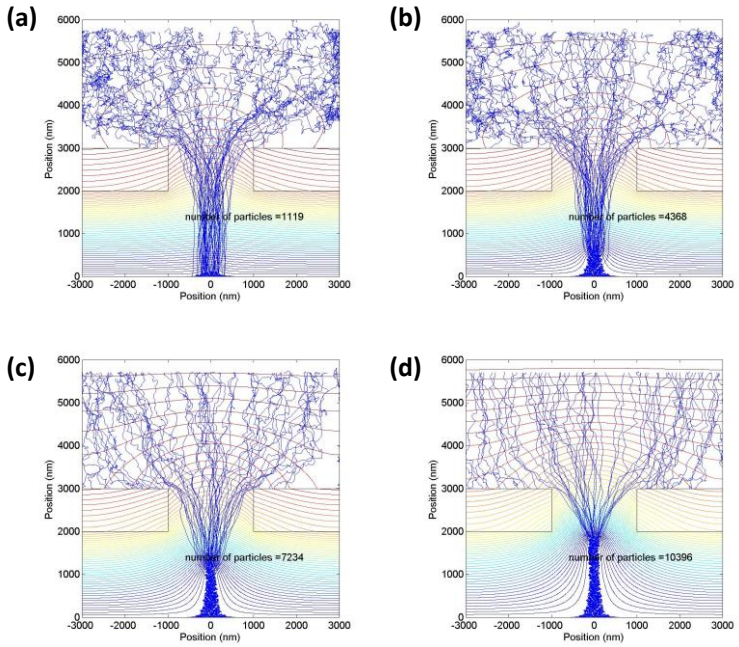

Figure 3.16. Simulation results for nanoparticle trajectories.

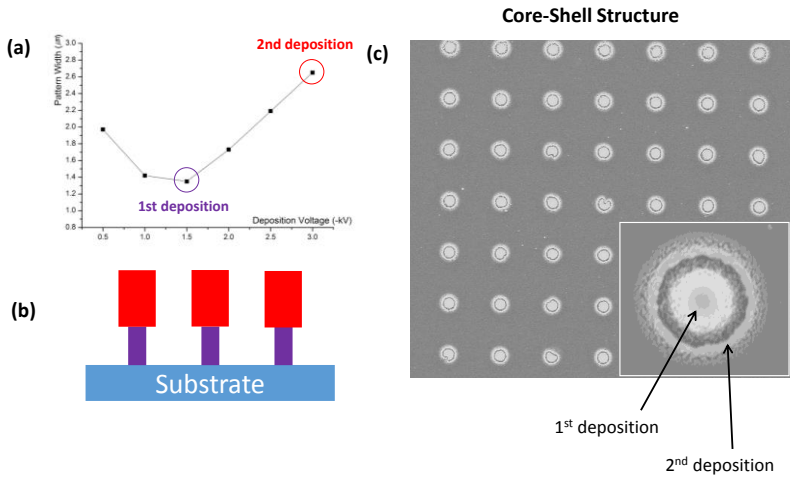

Figure 3.17. Core-shell structure fabricated by changing V_d from -1.5kV to -3.0kV during the nanoparticle deposition process (a) Nanoparticle deposition conditions

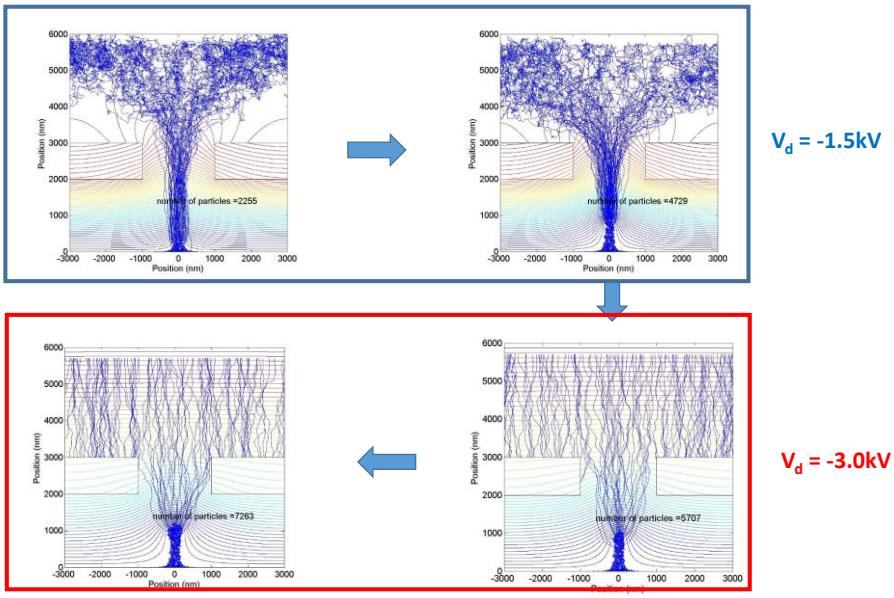

Figure 3.18. Simulation results for nanoparticle deposition. V_d was changing from -1.5kV to -3.0kV. The result shows that nanoparticles were deposited onto the structure even changing V_d. (inside red square)

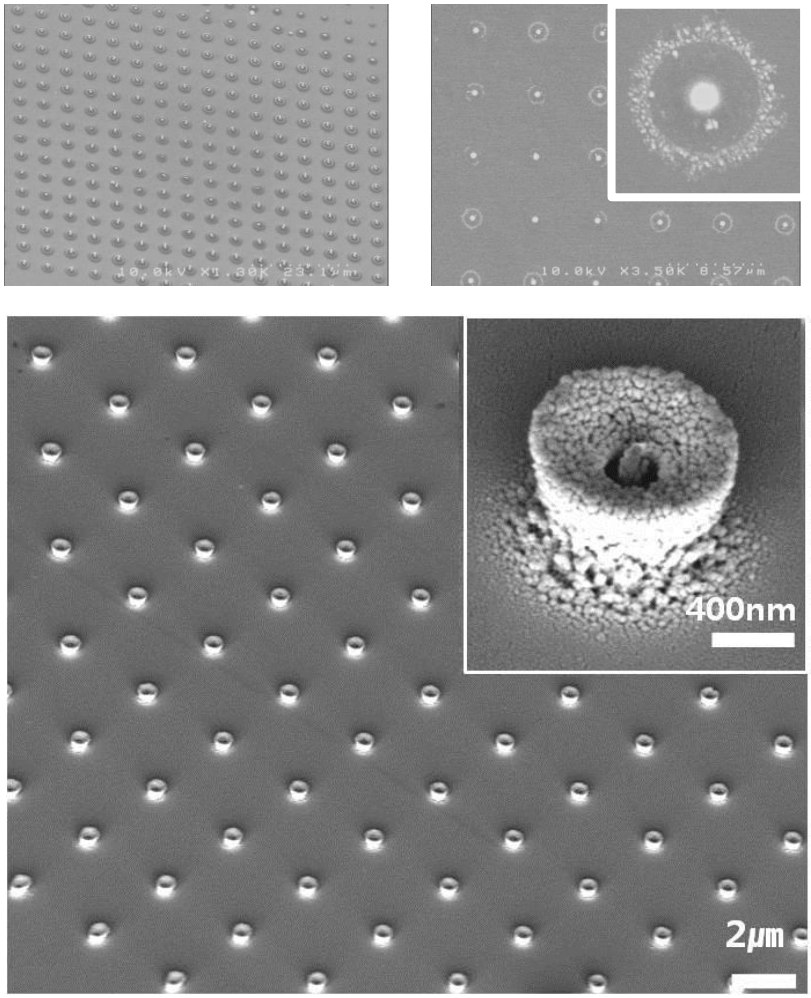

Figure 3.19. Various shapes of core-shell nanoparticle structures

3.6. Sequential deposition of various materials

Various materials can be pattered via IAAL, only if materials could be transformed in aerosol form. Furthermore, different materials can be used in single fabrication process.

Figure 3.20 shows nanowires consisting of Cu and Ag nanoparticles. Cu nanoparticles were deposited in 60mins firstly, then Ag nanoparticles were deposited in 20mins (V_i = -3.0k, V_d = -1.5 kV for both deposition) EDS analysis confirms 2 materials deposited in sequential

Figure 3.21 shows nanowires consisting of 2, 3 materials. **Figure 3.21(b)** shows that 3 materials could be used in consisting single nanowire.

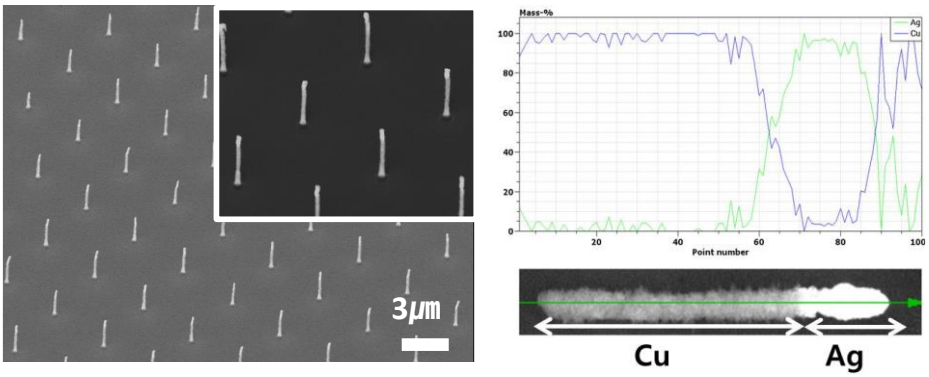

Figure 3.20. The fabrication of nanowires consisting of 2 distinct materials. Cu nanoparticle were deposited in 60mins, then Ag nanoparticle were deposited 20mins.

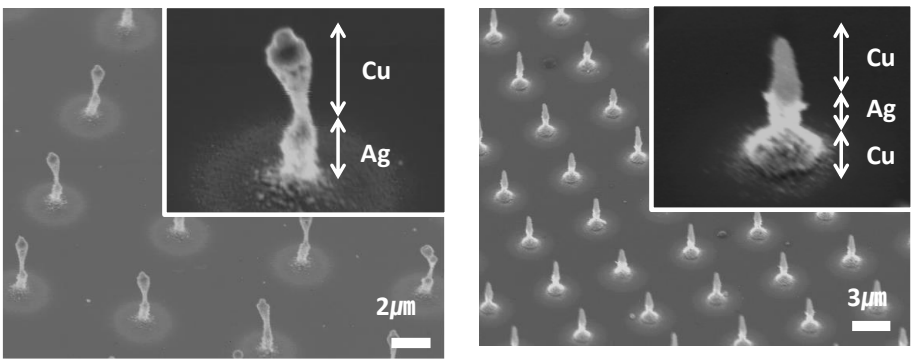

Figure 3.21. The fabrication of nanowires consisting of 2, 3 different materials. (a) Ag were firstly deposited in 40min, then Cu nanoparticles deposited in 40mins. (b) Cu and Ag were deposited time about.

3.7. Charge accumulation of the nanoparticle structure

The core-shell structure is extraordinary results which is inconsistent with the simulation result. (**Figure 3.17**) Since the same core-shell structure had been fabricated in repeat experiments, and nanoparticle trajectory simulations showed inconstant result with the experiment, we assumed the nanoparticle trajectory simulation might have problems.

Two assumptions were used in particle accumulation model. (**Figure 3.22**)

(1) Nanoparticles were conductive so when particles were deposited onto the substrate, all charges of the particle were neutralized.

(2) Nanoparticles had same potential with that of the substrate.

Based on these assumptions, electric field was calculated at each particle deposition step to update the potential changes with the growing of particle structure. It is noted that the potential of the cell with the particle was considered as V_d (assumption (2)), and the potential in the yellow box was only calculated. Therefore, the electric field near the top of the nanowire was high enough to attract the great part of charged nanoparticles and make nanoparticles deposited onto the structures. **Figure 3.16(a)** shows that trajectories of nanoparticles are toward to pre deposited nanoparticle cluster even in weak electrostatic lens effect. This phenomenon is called **"Antenna effect"**, as deposited nanoparticles acts like the antenna which attracts the other nanoparticle to be deposited onto the structure. The discrepancy between the experiment result and the simulation result is mainly due to this antenna effect. Therefore, new assumptions for Lattice models for Poission equation to weaken the antenna effect, was suggested. **Figure 3.24** shows new lattice model for Poission equation. 2 new assumptions were used;

(1) Nanoparticles were not considered as perfect conductor. So not every charges were neutralized, some charges still were accumulated in the structure.

(2) The potential of the cell with the nanoparticle was calculated by Poission equation. The electrical permittivity of the material of the nanoparticle was used to compute Poission equation.

In this new model, the cell with the nanoparticle was not excluded from the computation. Poission equation was computed in entire domain including the cell with the nanoparticle with electrical permittivity ε_2. And charges from the charged aerosol would not be fully neutralized, some charges still remained in the cell. Since the size of the nanoparticle used in experiments is under 10 nm, it was hard to tell nanoparticles are perfect conductor even material used to fabricate nanoparticles was metal. (Ag, Cu) And the nanoparticle structure consists of many nanoparticle, which means the structure has a lot of grain boundary. Therefore, it was reasonable to assume that not every charges be neutralized.

There was no reference of charge transfer on the nanoparticle structure, we simplified the assumption (1) by consider new factor, called charge accumulation probability Φ_c. The new model should satisfy 2 conditions.

(1) Nanoparticle structure had to grow straight if V_d is constant during the deposition process.

(2) Nanoparticle structure had the core-shell shape if V_d is charged during the deposition process.

The charge accumulation probability was acquired by try and error to satisfy the 2 condition.

If we used high Φ_c then, too many charges were accumulated inside the structure. As a result, the structure cannot be growth into the nanowire shape. (**Figure 3.25**) If we used low $\Phi_{c,}$ then the core-shell structure cannot be fabricated in case of changing high V_d (**Figure 3.18**). By try and errors, we found proper value of $\Phi_{c,}$ as 0.2.

Figure 3.26 shows nanoparticle trajectory simulation calculated with new assumption with $\Phi_{c,} =$0.2. Charged nanoparticles were deposited in nanowire shape even charges were not fully neutralized. Because of the electrostatic repulsion, some particles were deflected, then deposited at the side of the structure. **Figure 3.27** shows two results calculated from 2 different assumptions.

Charge accumulation inside the nanoparticle structure was examined by surface charge measurement experiment of charged nanoparticle film by KFM system.

We deposited copper nanoparticles generated by the spark discharge onto the silicon substrate in 120 mins. **Figure 3.28** shows Cu nanoparticle film deposited onto the silicon substrate. The substrate was fixed onto the substrate by the ceramic holder, so the thickness of the film is not uniform due to the electrostatic lens effect. The color of the film is changed depending on the thickness, which is observed in the optical image. The charge measurement was conducted at the region which had the thickness of 500nm. **Figure 3.29** shows surface potential measurement of Cu nanoparticle film. Even metal nanoparticles were deposited onto the conductive silicon wafer, charges were

not fully neutralized, stayed inside the film. The charge neutralized efficiency can be obtained by simple calculations. The electric potential above the charged plane is given by

$$V = \frac{\rho_s}{2\varepsilon_0}\left[(z^2 + b^2)^{\frac{1}{2}} - z\right]$$

where, z is distance between the plane and the point, ρ_s is surface charge density, and b is the radius of the plane.

Then we can calculate the neutralization efficiency of the charged nanoparticle film, which is 0.74. This calculation shows that 26% of charges still stay inside the nanoparticle film, which is consistency with the Φ_c=0.2 acquired by the nanoparticle trajectory simulation.

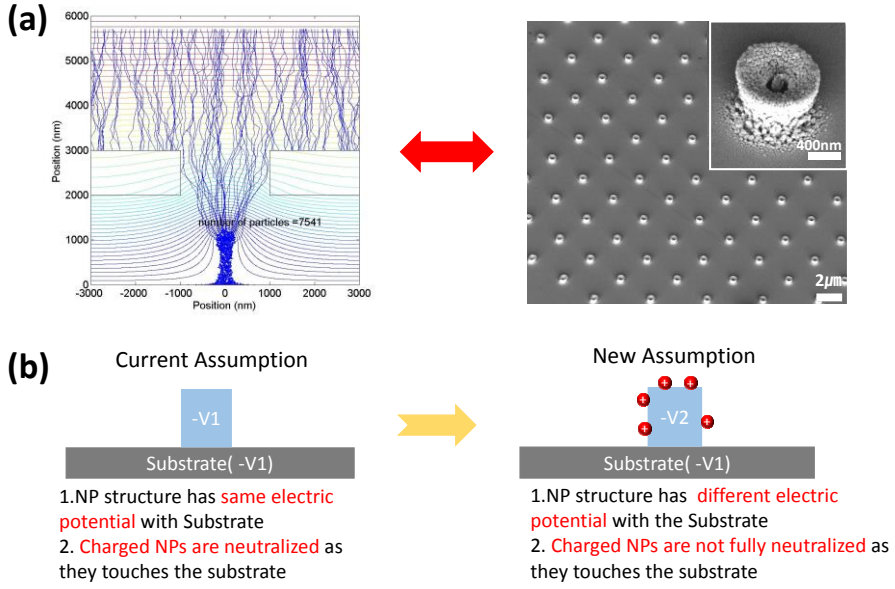

Figure 3.22. (a) The inconsistency between the simulation and the experiment. (b) New assumptions for the nanoparticle trajectory simulation.

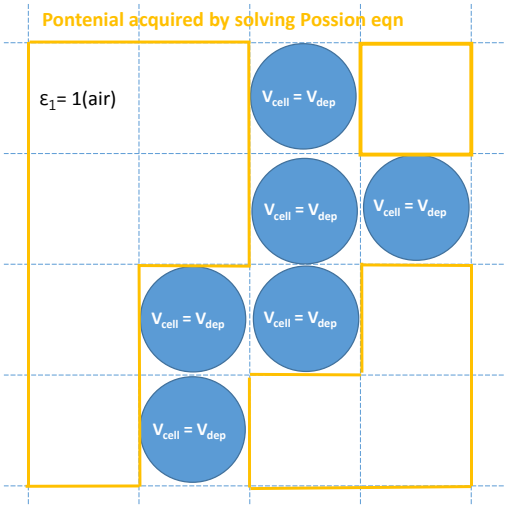

Figure 3.23. Lattice models for Poission equation. The potential of the cell with the particle was considered as V_d.

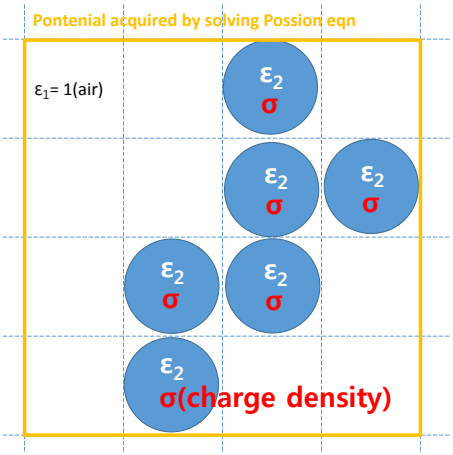

Figure 3.24. New lattice models for Poission equation. The cell with the particles has electrical permittivity ε_2.

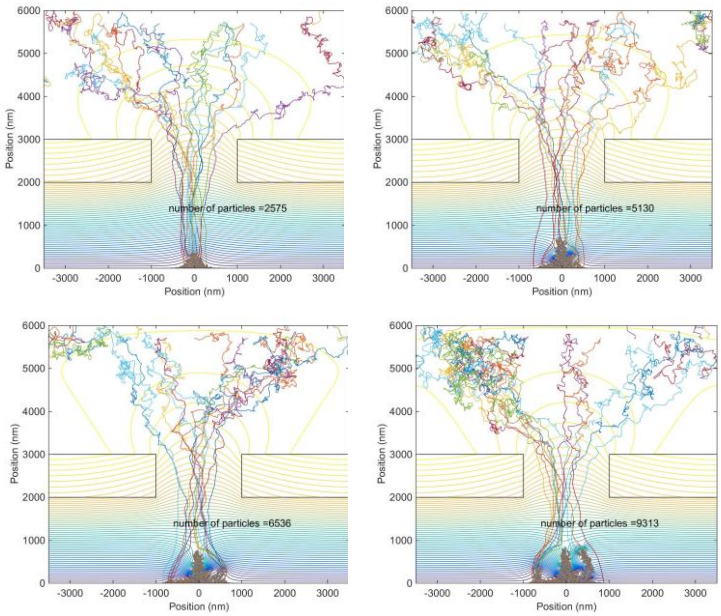

Figure 3.25. Nanoparticle trajectory simulation. With high value of Φ_c, nanowire structure cannot be fabricated due to charge accumulation.

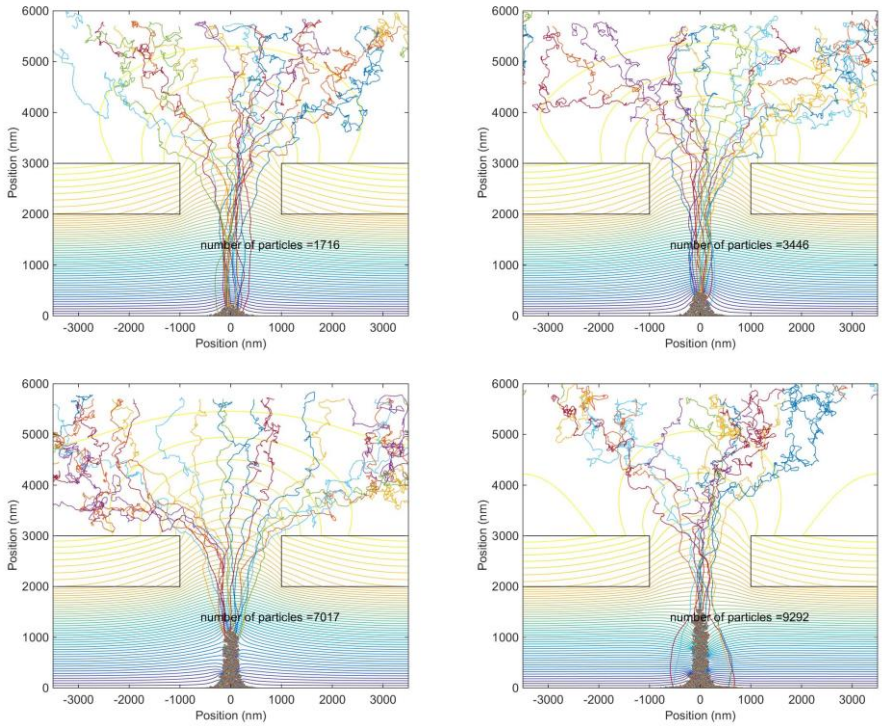

Figure 3.26. Nanoparticle trajectory simulation with $\Phi_c = 0.2$

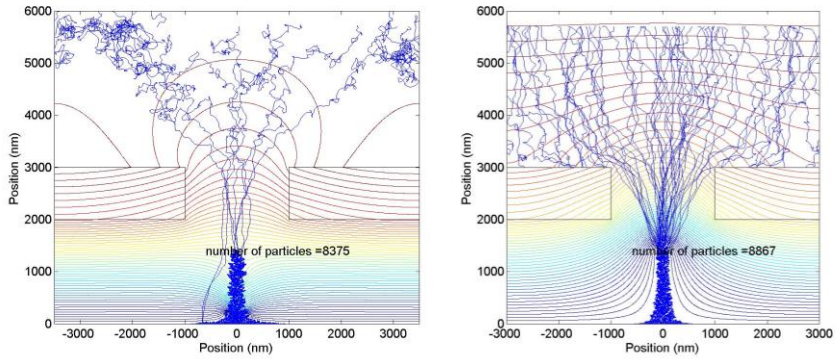

Figure 3.27. Comparison between nanoparticle trajectory simulation results.

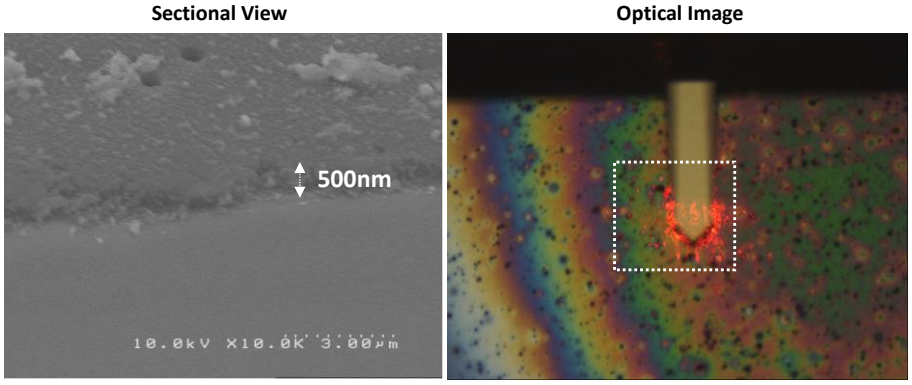

Figure 3.28. Cu nanoparticle film deposited onto the Si substrate. Cu nanoparticles were generated by the spark discharge method

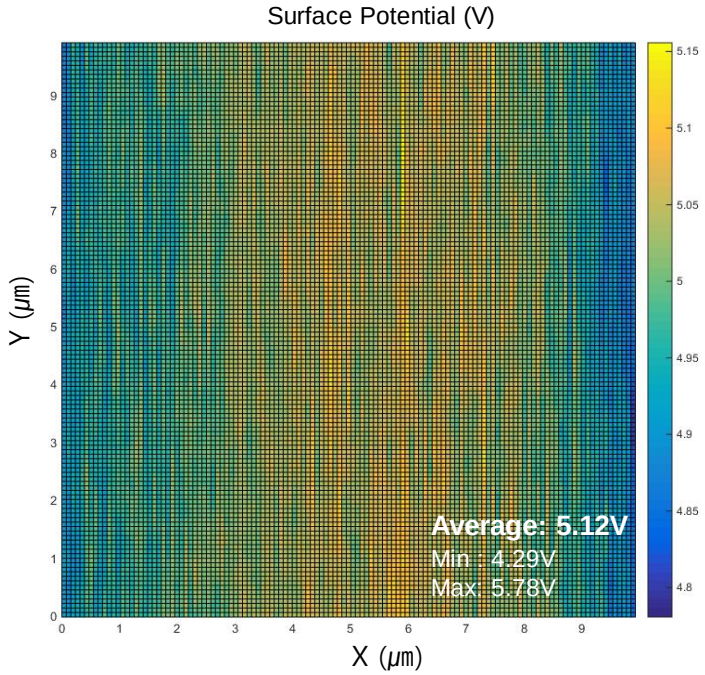

Figure 3.29 The KFM measurement result of Cu nanoparticle film

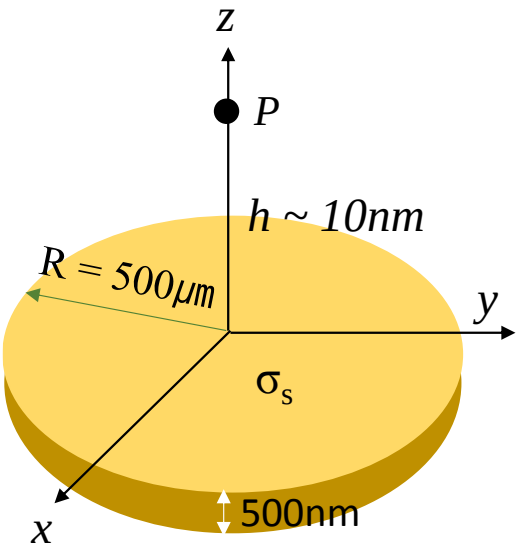

Figure 3.30 Simplified model for nanoparticle film

3.8. Conclusion

We studied factors affecting the electrostatic lens effect. 3 factors – ion accumulation voltage, deposition voltage, and mask-substrate distance – were closely examined and the experiment result was validated by nanoparticle trajectory simulation. In studying the effect of the deposition voltage, the discrepancy between the experiment and the simulation result was found and we figured out Brownian diffusion had influence on the nanoparticle motion in the low deposition voltage region.

By changing deposition voltage during the deposition process, the core-shell shape nanoparticle structure was fabricated and the mechanism of core-shell fabrication was examined

4. Controlled electrostatic focusing of nanoparticles using a charged floating mask

4.1. Introduction

Ion assisted aerosol lithography (IAAL) is an aerosol-based assembly technique, which utilizes the distorted local electric field induced by accumulated ions on pre-patterned substrate to manipulate the trajectory of charged NPs as they get drawn to the substrate by electrostatic attraction (Kim et al., 2006; Lee et al., 2009; Lee et al., 2010; Woo et al., 2011; Ha et al., 2014). IAAL uses ions that have accumulated on the photoresist (PR) pattern surface to induce the electrostatic lens effect which causes charged NPs to converge toward the center of the PR opening and deposit on the substrate underneath. To eliminate multiple PR patterning steps, a reusable non-conduction mask was fabricated from Si_3N_4 or epoxy to hold ions that induce the electrostatic lens effect (You et al., 2010). This mask can be used repeatedly since the NPs are selectively deposited onto the substrate, not on the mask, which eliminates the need to prepare a new mask for each operation. However, the ion accumulation on the mask surface should be precisely engineered for controlling the size of the printed patterns, which is not a trivial task. It is noted that electrostatic focusing occurred due to charged particle deposition on photoresist pre-patterns (Prost et al., 1998) or a Teflon mask (van der Eijk et al., 1973).

A method of applying an electric potential directly to the mask was proposed to induce electrostatic lens effect instead of using ion accumulation (You et al., 2008). Electrospun nanofibers have been focused within a few hundred micrometer range using the same concept (Salim et al., 2008) and carbon nanotubes (Marina et al., 2011) were similarly patterned within a few tens of micrometer range. Although these studies showed pattern size reduction of elongated nanomaterials such as nanotubes and nanofibers roughly up to a

few tens of micrometers range, a focusing control of a few nanometer sized nanoparticles within a sub-micrometer range was not demonstrated and a detailed particle trajectory analysis of charged aerosols was not carried out.

Here, we present a capability to precisely control the assembled NP cluster sizes by varying the applied potential difference between the mask and the substrate, enabling reliable printing of sub-micrometer sized patterns consisting of particles that are a few nanometers in diameter. First, it was computationally validated that electrified stencil mask causes similar electric field deformation to IAAL. Then, the effect of varying the applied potential difference between the mask and the substrate on the assembled NP cluster sizes was studied. Next, particle trajectory simulations were performed to confirm the NP focusing mechanism. Finally, a sequential deposition of silver and copper at distinct locations on the substrate was carried out to demonstrate versatility of this technique.

4.2. Fabrication of Electrified mask

Previously reported IAAL techniques used ions that have accumulated onto the insulating surface of the mask to generate electrostatic lens effect, which is illustrated in **Figure 4.1(c).** After placing a dielectric mask above the substrate, ions produced by corona discharges are injected and, deposited onto the surface of the mask. The accumulated ions create electrostatic lenses which make charged NPs converge into the centers of the mask openings (You et al., 2010). In comparison, **Figure 4.1(d)** shows a schematic overview of the NP assembly technique used in this work. In this method, ions are not needed, instead, the electrified metal coated mask is located apart from the Si substrate to generate electrostatic lens effect. The produced charged NPs were injected into the deposition chamber where a platinum coated Si_3N_4 stencil mask and a Si substrate had been installed and separated by 4 μm using a nano-positioning stage. These particles followed the electric field streamlines induced by the potential difference applied to the mask and the substrate, and were eventually deposited onto the substrate. The 1 μm thick Si_3N_4 stencil mask was fabricated by coating a Si wafer with a 1 μm thick low stress Si_3N_4 film and patterning it using photolithography and eliminating bottom Si layer via reactive ion etching process. The top surface of the stencil mask was coated with a 100 nm thick Pt film by sputtering. A high-voltage power supply (FuG Elektronik GmbH, HCP 140-12500) was used to apply constant voltages to the mask and the substrate separately.

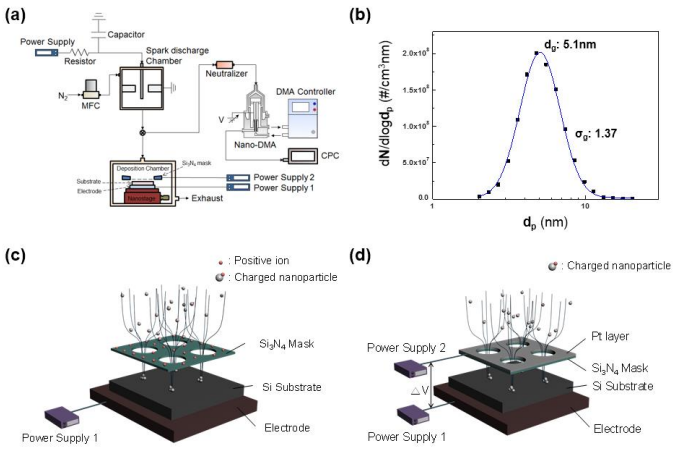

Figure 4.1. (a) Experimental setup consisting of a spark discharge chamber, an ESP and a SMPS. (b) Size distribution measured by an SMPS. Schematic representations of nanoparticle assembly methods by (c) ion accumulation and (d) voltage difference between the substrate and the metal coated mask.

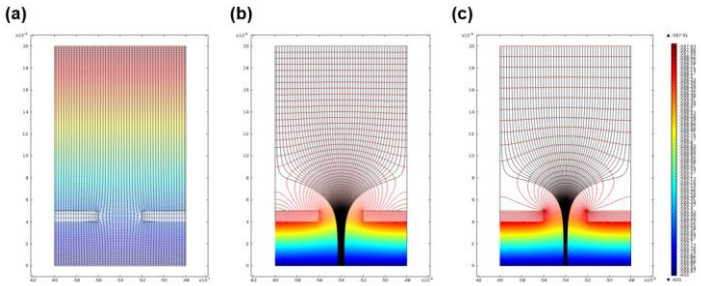

Figure 4.2. Electric field simulation results for various boundary conditions at the mask surface, (a) none charge (b) ion accumulated surface charge density (5.3×10^{-6} C/m^2) (c) electric potential difference between the substrate and the mask layer (2.0 V)

4.3. Electrostatic lens effect induced by an electrified mask

Figures 4.2(a), **(b)**, and **(c)** show the results of the electric field simulations for various experimental conditions. When there is no potential difference between the mask and the substrate, the electric field is uniform across the mask opening (**Figure 4.2(a)**). However, when ions are accumulated on the mask, they deform the electric field and generate an electrostatic lens effect that focuses electric field streamlines into the center of the mask opening (**Figure 4.2(b)**). When a voltage is applied directly to the mask surface, the potential difference (2.0 V) between the mask and the substrate creates a very strong electric field underneath the mask (4.7×10^5 V/m) which is much stronger than the electric field above the mask (1.03×10^4 V/m). Hence, the equipotential lines get distorted from linear alignment parallel to the substrate to concaving toward the substrate near the mask opening (**Figure 4.2(c)**). The resulting electric field streamlines take very similar forms to those generated in the ion accumulation case. Thus, applying a voltage directly to the mask surface creates similar electrostatic lens effects to ion accumulation on the mask surface.

4.4. Controlled focusing of nanoparticles

To quantify and compare the extent of focusing of nanoparticles for different experimental conditions, we define a parameter called 'focusing ratio (FR)' to be the ratio of the mask opening size to the patterned NP cluster size. The top panel of **Figure 4.3(a)** shows the line-patterned mask, and the bottom panel shows the charged Ag NPs deposited through the mask. The gap between the mask and the substrate was set to be 4 μm, and the voltage applied to the mask and the substrate were -598 V and -600 V, respectively. It was found that the pattern width of the deposited Ag NPs is 600 nm, which corresponds to a FR of 6.7. **Figure 4.3(b)** shows 550 × 550 nm2 square pattern consisting of Ag NPs, obtained via a stencil mask with 4 × 4 μm2 square openings (inset image of **Figure 4.3(b)**), which corresponds to a FR of 7.3. These results show that our approach has similar focusing performance to IAAL, which generally shows FRs ranging from 4 ~ 20 (You et al., 2010).

An important advantage of this approach is that the FR can be easily controlled by adjusting the potential difference between the mask and the substrate. **Figure 4.3(c)** shows the change in the NP cluster width depending on the potential difference between the mask and the substrate. The voltage applied to the substrate was fixed at -600 V while the voltage applied to the mask was varied at -599.5 V, -599.0 V, -598.0 V and -597.0 V. The cluster width decreased from 2 μm to 600 nm which corresponds to FRs of 2 to approximately 6.7. As the potential difference increases, the electric field below the mask gets stronger, resulting in a rapid change in the electric field strength from the top side to the bottom side of the mask. Therefore, the distortion of the equipotential lines increases, causing the electric field lines to become more focused. The charged

NPs travel along the field lines and get deposited, therefore the cluster width decreases as the potential difference increases, which indicates that FR can be controlled by simply adjusting the potential difference applied between the mask and the substrate. This would be a more robust way to control the focusing of charged nanoparticles than by using ion accumulation. The Brownian uncertainty calculated in this setup was approximately 800nm. As a result, increasing potential difference more than 5V was useless because the pattern width could not be decreased due to the Brownian diffusion. (**Figure 4.5**)

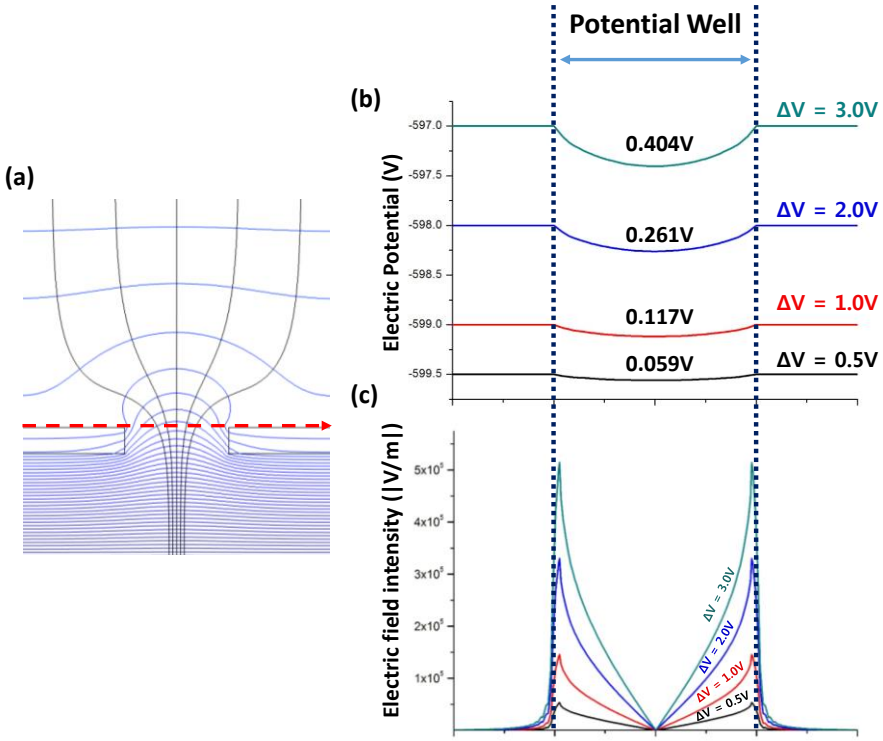

Figure 4.3. Electric potential along the mask surface. Dotted blue line represents the opening of the mask.

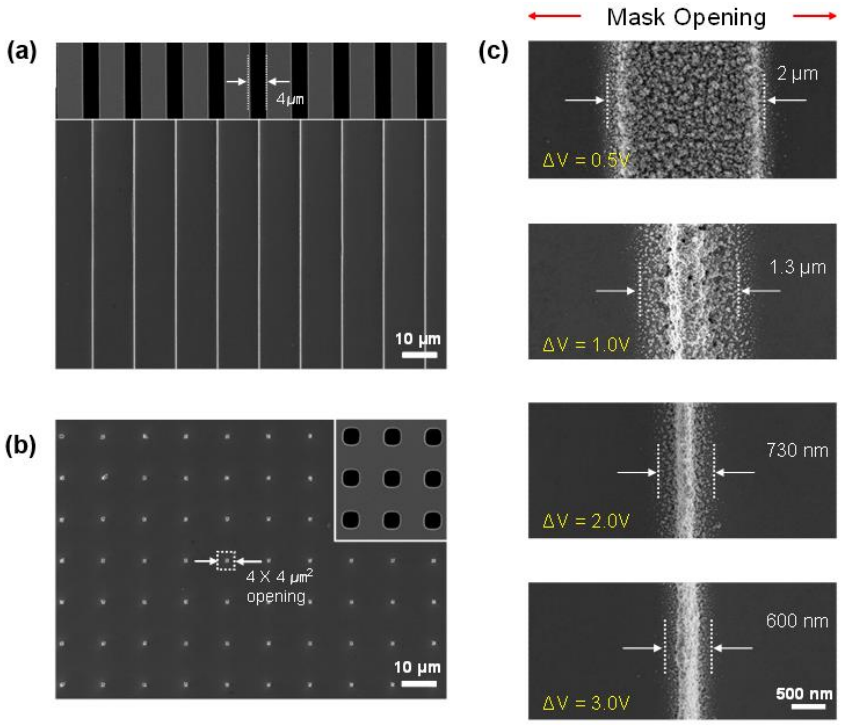

Figure 4.4. (a) Images of metal-coated mask (above) and patterned Ag nanoparticles deposited through the mask (below). (b) Pattering Results of Ag nanoparticles through a mask with square openings (inset image). (c) Effect of the potential differences on the pattern width; from top to bottom, the potential differences applied are 0.5 V, 1.0 V, 2.0 V and 3.0 V

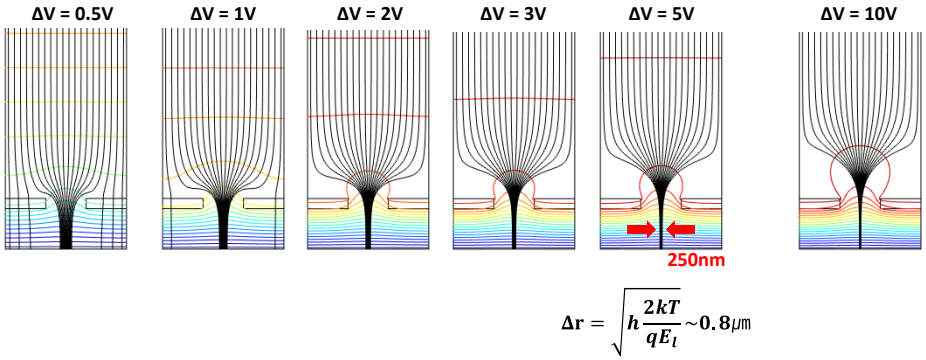

Figure 4.5. Electric field simulation results depending on voltage differences between the mask and the substrate

4.5. Particle trajectory simulations

The potential differences between the metal layer and the substrate used in the simulations were the same as the experimental conditions ranging from 0.5 V to 3.0 V. Before the charged particles approach the mask, their trajectories are dominated by their Brownian motion. However, when the charged particles travel closer to the mask, they are drawn into the mask openings by electrostatic attraction to the substrate. 150 particles were introduced for each simulation and the distribution of the particles' final deposition locations was estimated by fitting with a Gaussian distribution (**Figure 4.6(b)**). The full width at half maximum (FWHM) values of the fitted profiles was chosen to represent the cluster width from the simulations. The FRs from the simulations ranged from 2.5 to 6.2 while the values from the experiments ranged from 2 to 6.7. The simulation results showed the same tendency as the experimental results, FR increasing as the applied potential difference increases. The particle trajectory simulations were shown to predict the FRs with reasonable accuracy and

confirmed that the electrostatic lens effect can be controlled by adjusting the potential difference between the mask and the substrate.

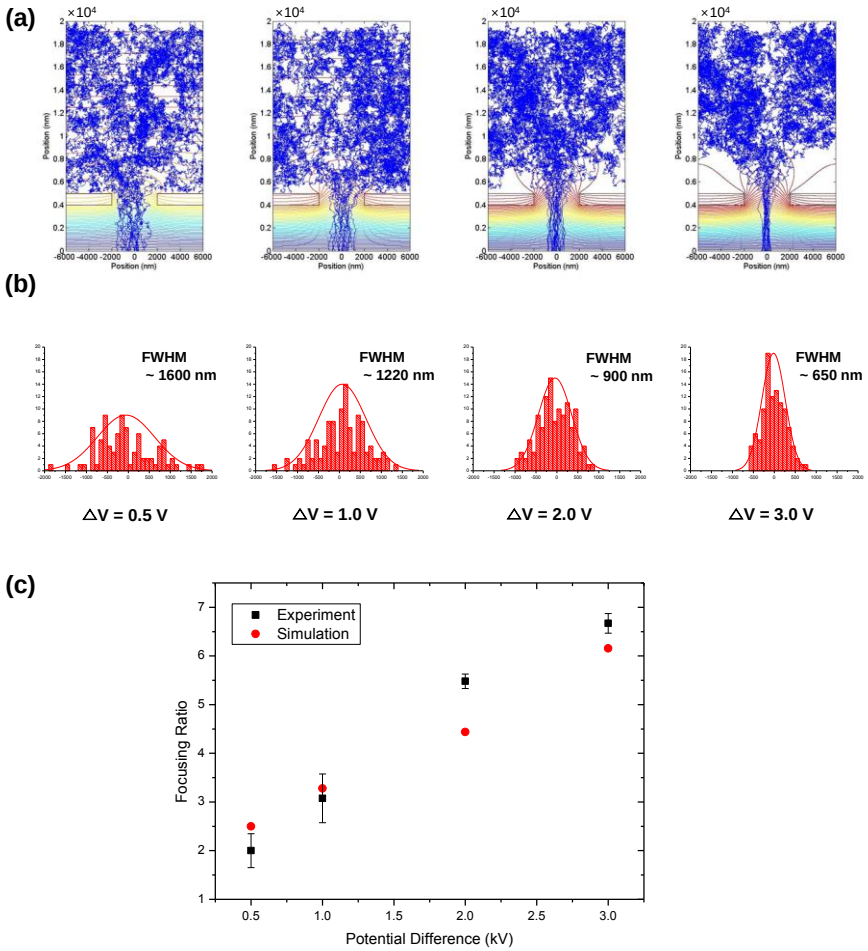

Figure 4.6. Simulation results for (a) particle trajectories and (b) corresponding histograms for the final particle deposition locations depending on the potential differences between the substrate and the metal layer [0.5 V, 1.0 V, 2.0 V, and 3.0 V] (c) The variation of the FR values as a function of the applied potential difference.

4.6. Sequential deposition of multiple materials

To exploit the fact that NPs are deposited locally through the mask which is installed at a fixed distance from the substrate, the mask could be translated after one deposition for sequential deposition of various materials without damaging the previously deposited NP clusters or the substrate. **Figure 4.7(a)** shows that silver and copper particles are deposited sequentially in distinct locations after offsetting the mask. In this experiment, silver and copper NPs were generated by spark discharge method and the mask was translated laterally by 4 μm between depositions. **Figure 4.7(b)** shows the result of an energy-dispersive X-ray spectroscopy (EDS) analysis, which confirms that the two different materials are deposited separately at desired locations on the substrate.

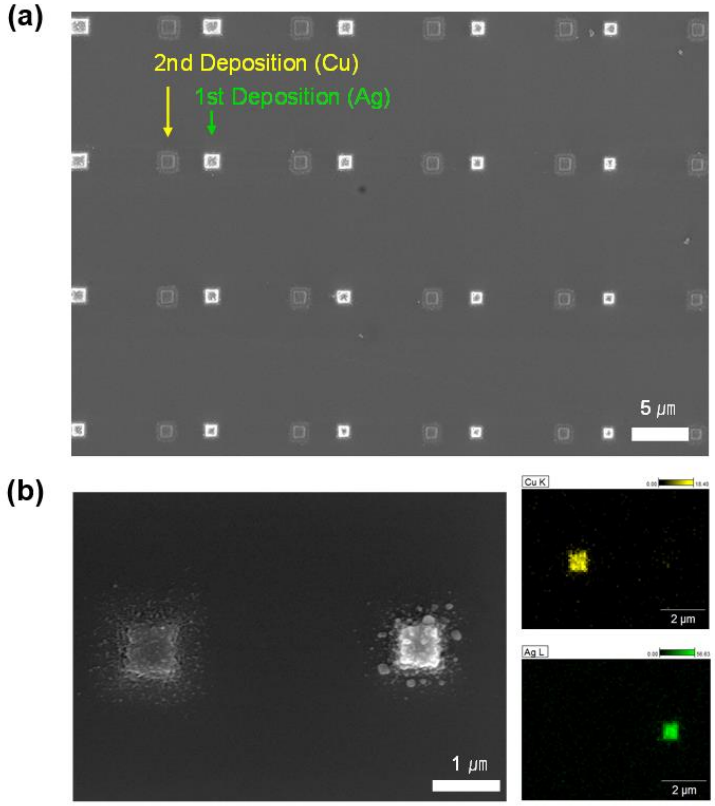

Figure 4.7. (a) Offset multi-material nanoparticle cluster array formation using mask translation. (b) EDS images of nanoparticle clusters confirming successful fabrication of silver and copper nanoparticle clusters without intermixing of the constituent materials.

4.7. Conclusion

We have expanded the principle of ion-induced focusing to controllably reduce pattern dimensions via a floating metal coated stencil mask by applying an electric potential. We have demonstrated experimentally and numerically that the ratio of focusing of nanometer-sized particles can be easily controlled from 2 to 6.7 by adjusting the applied potential difference between the floating mask plate and the substrate and successfully produced submicron patterns of particles using a mask with micrometer-sized openings. The focused NP deposition mechanism was elucidated through particle trajectory simulations performed by solving the Langevin equation. The results of the simulations are in good agreement with the experimental data. We have also demonstrated the versatility of this technique by creating multi-material offset NP cluster arrays by assembling silver and copper NP clusters separately at desired locations.

5. Dynamic 3D nanoparticle assembly via translating a floating mask

5.1. The mask-substrate installation

Basic experiment conditions such as the nanoparticle generation, fabrication of stencil mask was consistent with previous experiments. But now the relative location between the mask and the substrate was changing during the nanoparticle deposition process for 3D active nanoparticle printing. The mask was fixed to the deposition chamber at fixed location, while the substrate was translated by 3D piezo-actuated stage. The piezo-actuated stage was controlled by closed-loop feedback system, so the accuracy of the stage was 4nm.

The difficult part of the experiment setup was to parallel alignment between the mask and the substrate. As we already discussed in Chapter 2, the focusing effect was determined the distance between the mask and the substrate. So parallel alignment should be guaranteed for the uniform patterning of nanostructure. In previous experiments, there was no need of relative moving between the mask and the substrate, so the mask and the substrate was fixed by the ceramic holder. But in this experiments, precise controlling of relative translation between the mask and the substrate was important, different methods had to be considered. The substrate was fixed onto the substrate by silver paste. Then, the mask was placed above the substrate, which was for parallel alignment between the mask and the substrate. The mask was attached on the mask holder with the polymer glue. After curing the polymer glue for 30mins, the distance between the mask and the substrate was controlled by piezo-controlled stage.

5.2. Sequential Deposition of Nanoparticles

Figure 5.1 shows nanoparticle structures deposited sequentially in distinct locations after offsetting the mask. **Figure 5.1(b)** shows the firstly deposited nanoparticle structure deposited in 90mins. The second structure was fabricated after translating the mask in 4 μm. The second structure in **Figure 5.2(c)** was deposited in 60mins and in **Figure 5.2(d)** was deposited in 90mins. **Figure 5.2** shows the sequential deposition of line patterned silver nanoparticles. The mask was translated by 1 μm, and the deposition time was 40mins for both structure. These results shows that the translating the mask do not affect the firstly deposited nanoparticle structure and the nanoparticle focusing effect also was not affected by the firstly deposited nanoparticle structure. The antenna effect originating from the first structure was hindered by ions deposited on the mask surface. So the focusing effect was affected solely by process parameters in 2nd deposition process.

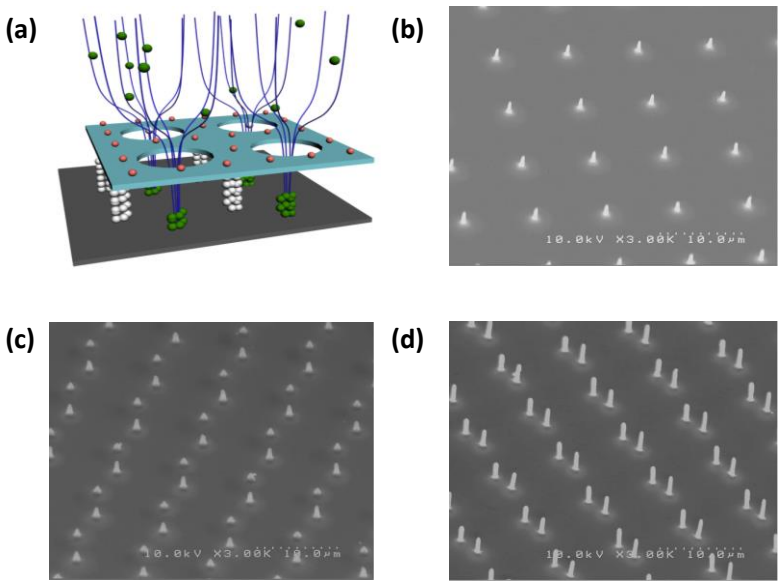

Figure 5.1. Offset multi-material nanoparticle cluster array formation using mask translation

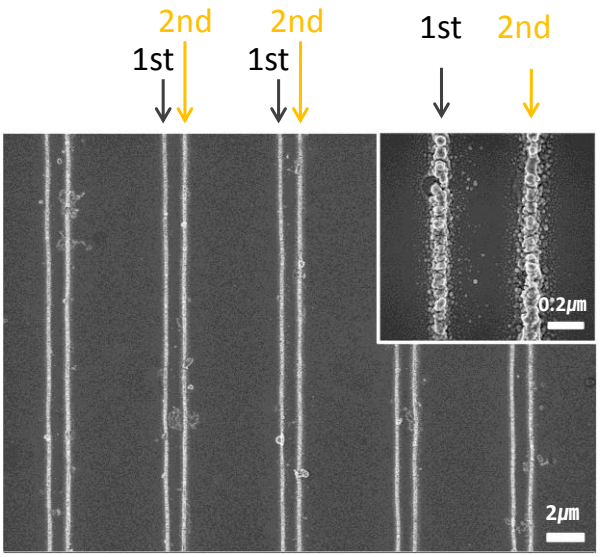

Figure 5.2. Line patterned nanoparticle structure using mask translation

5.3. Fabrication of high aspect ratio nanostructure

The nanowire with the high aspect ratio can be fabricated by translating the mask in vertical direction. When nanoparticle structure was overgrown above the mask, the shape of structure was changed in mushroom shape due to the antenna effect. So the length of nanowire was restricted by the distance between the mask and the substrate.

Therefore, to fabricate high aspect ratio nanowire, the distance should be increased. However, the uncertainty **Δr** was getting increased because the total translating distance **r** was increased as the distance between the mask and the substrate increased.

The high aspect ratio nanowire could be fabricated by translating the mask in vertical direction while keeping depositing nanoparticles. Moving the mask in vertical direction with the same velocity of the growth rate of nanoparticle structure, nanoparticles were keeping deposited on the structure with maintaining short total translating distance. **Figure 5.3** shows the high aspect ratio nanowire fabricated by translating the mask in vertical direction. Total deposition time was 180mins.

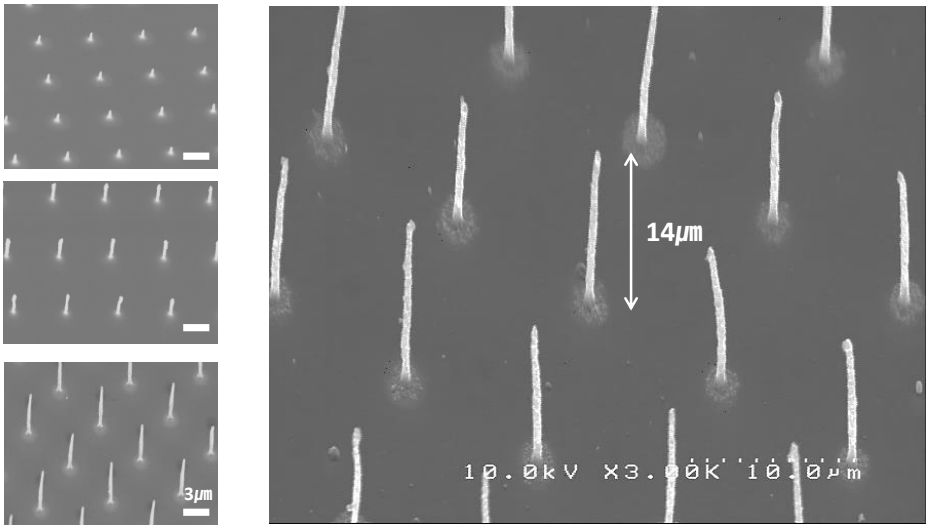

Figure 5.3. High aspect ratio nanowire fabrication by translating the mask in vertical direction

5.4. Active fabrication of 3D nanoparticle structure

In previous, nanostructure array was fabricated by sequential deposition of nanoparticles. After finishing fabrication of first nanostructure, the mask was translated then, second nanostructure was fabricated. In this time, now the mask was being translated during nanoparticle deposition process. The shape of nanoparticle structure is now determined not by the shape of the mask opening, but the trajectory of the mask transition, which is like 3D printing technique.

Because of the antenna effect of the nanostructure, charged nanoparticles are attracted to the shape tip of the structure. As a result, nanoparticles tend to moving toward the nanostructure, even the center of the mask opening is not aligned with the nanostructure. Consequently, the shape of the nanostructure can be controlled by trajectory of the mask translation. If the nanoparticle cluster is too small to induce the antenna effect, charged nanoparticles are deposited beside the deposited cluster, which likes nanoparticle writing. So the mask translation velocity is important parameter to determine whether the process is 3D printing or 3D writing. **Figure 5.4** shows the schematics of nanoparticle structure fabricated in the transition condition between the 3D printing and 3D writing. In the 3D printing mode (slow translation), charged nanoparticles were continually deposited onto the top of the structure, so tilted nanowire was fabricated by slow translation. (Figure 5.5(a)) In the writing mode in the other hand, the mask is translated fast, so charged nanoparticles were deposited beside previously deposited nanoparticle cluster. (Figure 5.5(b))

In this reason, it is important to choose proper mask translation speed for fabricating intended shape of nanoparticle structure. To find translation speed

for separating the 3D printing and nanoparticle writing, nanoparticles were deposited with various mask translation speed.

Figure 5.6 shows nanoparticle cluster fabricated with translating mask in 2 μm with 80 minutes. Some portions of structure grew in 3D structure, while the others were deposited in writing mode. With this result, we assumed that speed of 2μm/80minutes was the criteria for separating the 3D printing and nanoparticle writing.

Figure 5.7 shows the nanoparticle cluster fabricated by translating the mask in writing mode. In writing mode, the deposition time to complete the movement was short, the cluster size of the deposited nanoparticle was small. So to fabricate the enough size of the nanoparticle structure, the mask was translated repeatedly with the same trajectory to increase the total deposition time. The translation distance was 4 μm and the deposition time was total 50mins while 5 repetitions with same trajectory. Particles were deposited uniformly following the trajectory, no antenna effect could occur during the nanoparticle deposition process. The nanoparticle wall can be fabricated by increasing the deposition time and repeat times.

Figure 5.8 shows that various nanoparticle cluster by nanoparticle writing method.

When the translation speed is sufficiently low, nanoparticles were deposited in nanowire shape, which is 3D printing mode. Now the antenna effect could appear near the nanoparticle structure, charged nanoparticles were attracted toward the top of the structure and deposited onto. In this 3D printing mode, nanoparticles were deposited onto the top of the structure, the trajectory of the mask translation determine the 3D shape of product.

Figure 5.9 shows the 3D nanoparticle structure fabricated by 3D printing mode. Total translation distance was 2 μm and deposition time was 100 minutes. At the first stage of deposition process, the mask was not translated to make the enough size of nanoparticle cluster for induce antenna effect. After initial deposition in 40mins, the mask was translated 2 μm with 60mins. Growing direction of the nanoparticle structure was changed with the translation of the mask, which indicate that 3D nanoparticle structure could be produced as the trajectory of the mask.

Figure 5.10 shows various shape of 3D nanoparticle structure fabricated by 3D printing mode. Shape of the structure was determined by mask translation, and the tilted angle of the structure was determined by α; With high value of α, tilted angle of the structure was high and with the low value of α, the structure is almost tangential to the substrate.

As the mask translation speed was an important factor affecting the geometry of the structure, it is necessary to examine the shape of the structure with changing the translation speed.

Figure 5.11 shows nanoparticle structure fabricated with diverse translation speed. The geometry of the nanoparticle structure was varied depending on the translation speed. But not only the translation speed is matters, but nanoparticle supplement is also important factor. While maintaining same mask translation speed, increasing the particle supplement has the equal effect with reducing the translation speed and vice versa. Consequently, both the mask translation speed and amount of particle supplement should be considered to separate the 3D printing mode and writing mode.

We developed the new variable called modified mask translation speed α which was defined ratio between the mask translation speed and the vertical growth rate of nanoparticle structure.

$$\alpha = \frac{u_{mask}}{r_{VG}}$$

where u_{mask} is the mask translation speed and r_{VG} is the vertical growth rate of the nanoparticle structure.

The vertical growth rate can be obtained by dividing total particle supplement consisting of nanoparticle structure with cross section area of the structure

$$\text{Vertical grwoth rate}\left[\frac{\text{m}}{\text{s}}\right]$$

$$= \frac{Collection\ \ efficiency(\varepsilon)[\%]\ \ \times Nanoparticle\ \ Supply\ \ \left[\frac{m^3}{s}\right]}{Cross\ \ section\ \ area\ \ of\ \ structure\ \ [m^2]}$$

$$= \frac{Collection\ \ efficiency(\epsilon)[\%] \times Volume\ \ Fraction(\emptyset)\left[\frac{nm^3}{cm^3}\right] \times Flow\ \ rate(Q)[\frac{m^3}{s}]}{Opening\ \ area\ \ of\ \ unit\ \ pattern\ \ (A_p) \times Focusing\ \ ratio}$$

It is difficult to calculate the focusing ratio analytically, so we made simple assumptions which are (1) charged nanoparticles follow the streamline of the electric field and (2) Density of the electric field is proportional to electric field intensity. In these assumptions, focusing ratio can be obtained by comparing the electric field intensity between upper and lower the mask.

$$E_{avg.upper} = \frac{V_{mask}}{d}$$

$$E_{avg.lower} = \frac{V_{sub} - V_{mask}}{h} = \frac{\Delta V}{h}$$

where $E_{avg.upper}$ is average electric field intensity above the mask and $E_{avg.lower}$ is average electric field intensity below the mask. Actual electric field intensity is not uniform, but we use average values for convenience of the calculation. Now we can calculate the focusing ratio,

$$\text{Focusing ratio} = \frac{h \cdot V_{mask}}{d \cdot \Delta V}$$

Combining obtained variable into the modified mask translation speed α

$$\alpha = \frac{u_{mask}}{r_{VG}} = \frac{u_{mask}}{\epsilon \emptyset Q} \frac{A_p h}{d} \frac{V_{mask}}{\Delta V}$$

Applying α into **Figure 5.11**, we have changes of the nanoparticle structure considering every process variable which is depicted **Figure 5.12**. From repeated experiments, we found that α=1.5~3 is the boundary which separate the 3D printing mode and writing mode.

In writing mode, the deposition time was relative short to fabricate enough size of the nanoparticle structure.

In 3D printing mode, the tiled angle of the structure is determined by speed of the mask translation. With high α, the angle of the structure was small, and

low α, the structure is growing tangentially with the substrate. To fabricate very tilted structure, α should be high enough. But α cannot be exceed the boundary between the 3D printing mode and writing mode. This problem can be solved by double stage mask translation; first, nanoparticles are deposited with staying the mask to fabricate the nanoparticle cluster which can induce the enough antenna effect. After the forming the nanoparticle cluster, the mask is translating with high α to fabricate very tilted structure. Even with high α value, strong antenna effect makes charged nanoparticle attracted toward to the nanoparticle cluster and deposited onto. Eventually highly tilted nanoparticle structure can be fabricated. **Figure 5.13** shows highly tilted nanoparticle structure by above explained method. At the initial deposition stage, the mask was not moved in 20mins, then the mask was translated in 2 μm.

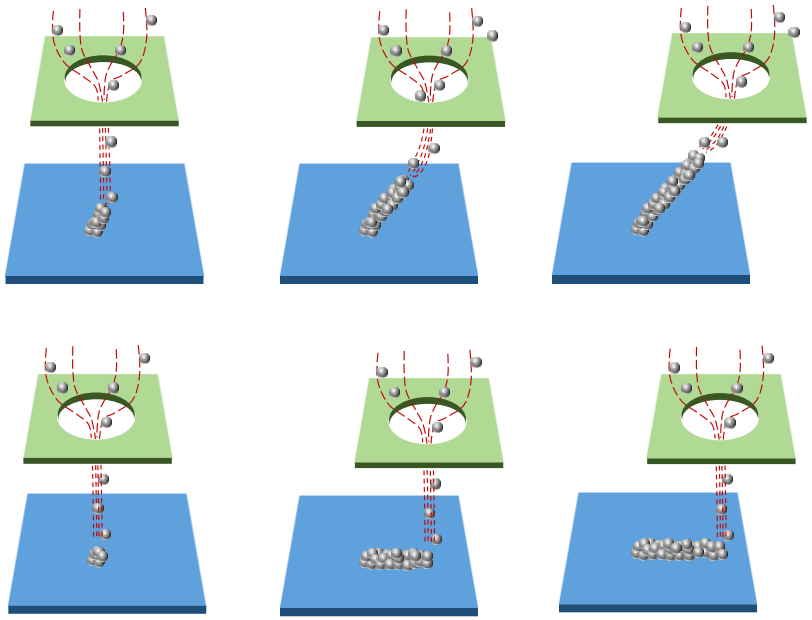

Figure 5.4 Schematics of 3D printing (upper) and nanoparticle writing (lower)

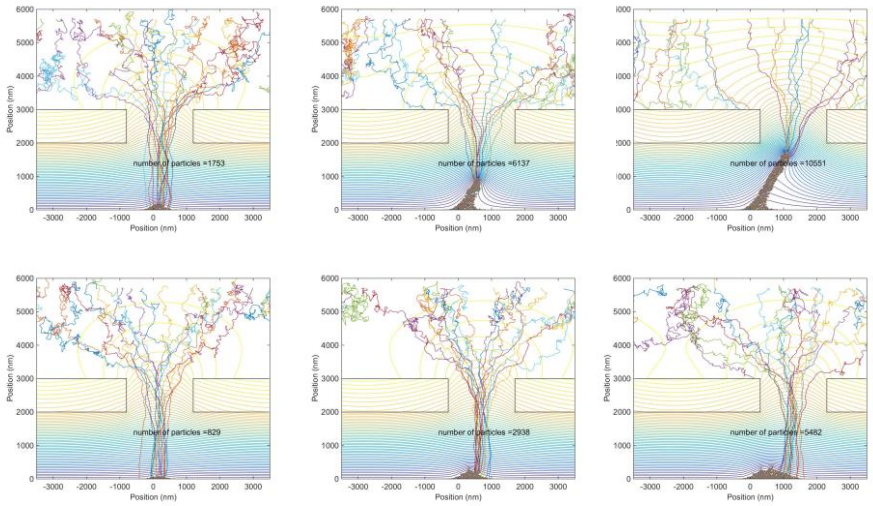

Figure 5.5. Nanoparticle trajectory simulation for 3D printing (upper) and nanoparticle writing (lower)

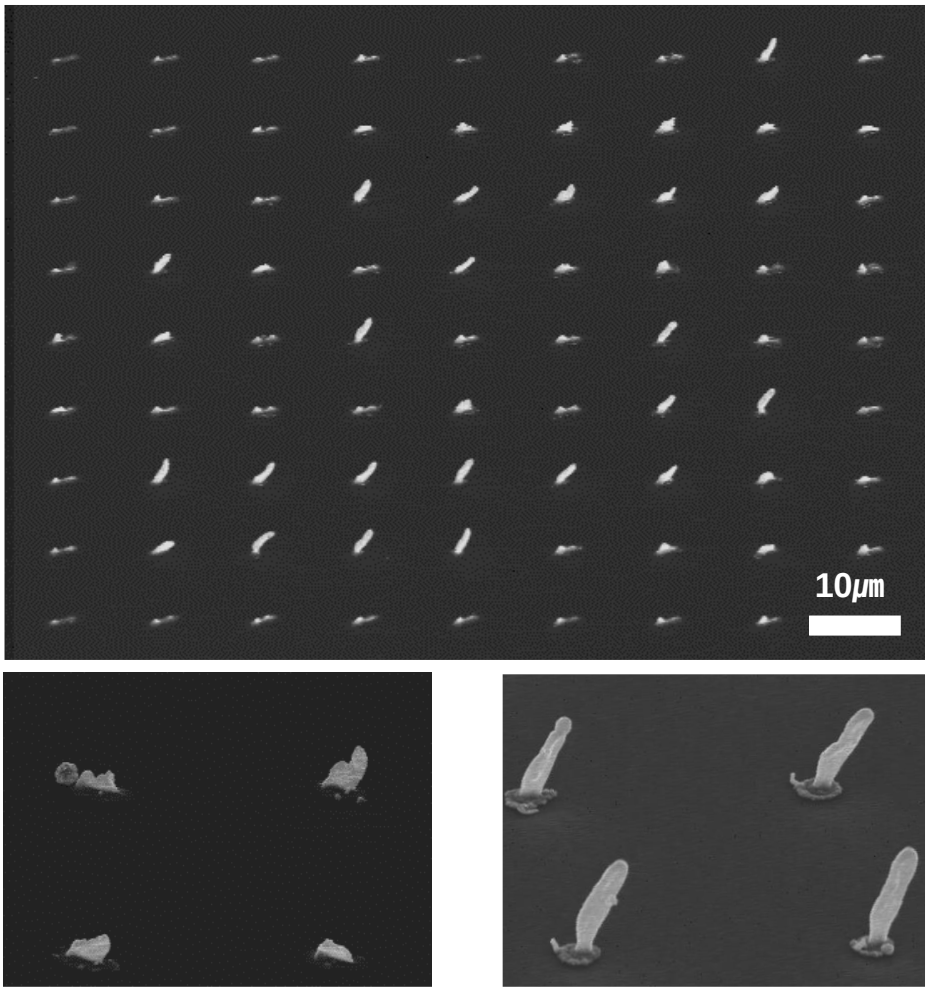

Figure 5.6. Nanoparticle cluster fabricated in the condition of division between 3D printing and 3D writing

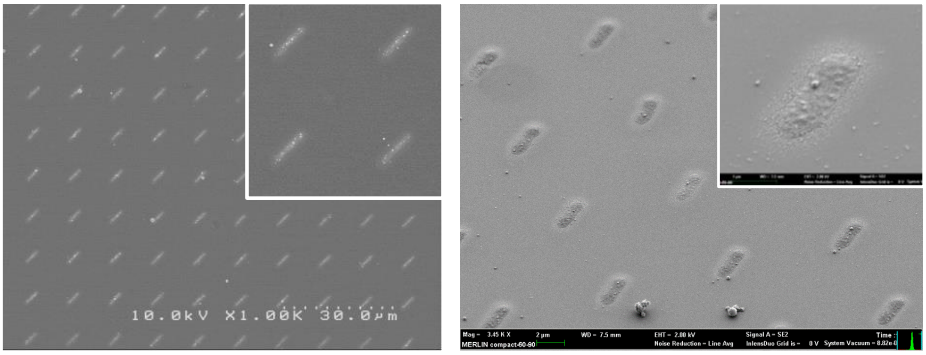

Figure 5.7. Nanoparticle cluster by nanoparticle writing

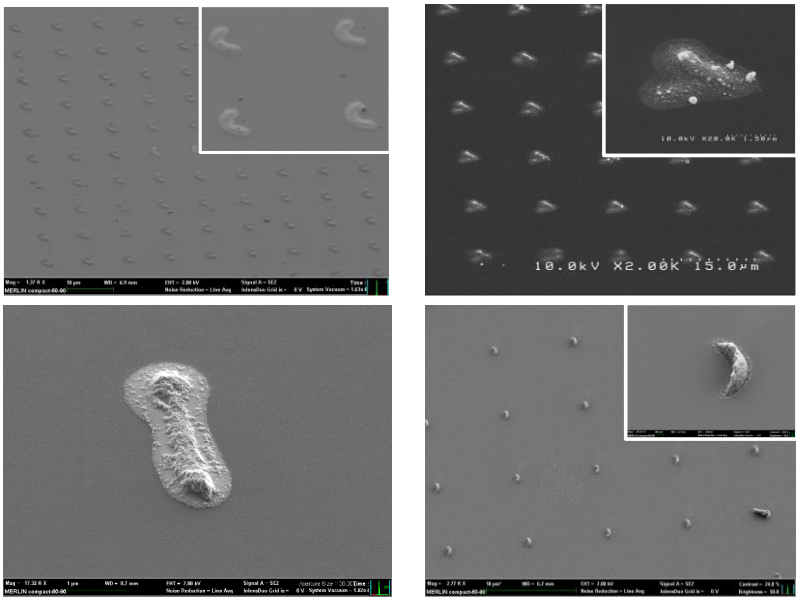

Figure 5.8. Various nanoparticle cluster fabricated by nanoparticle writing.

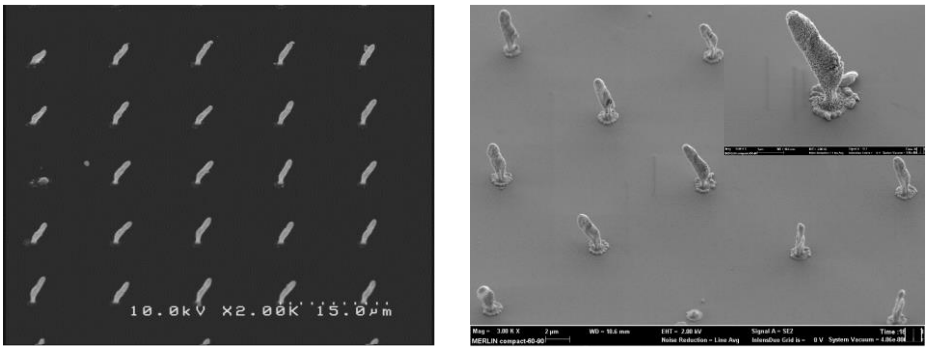

Figure 5.9 3D nanoparticle structure fabricated by 3D printing

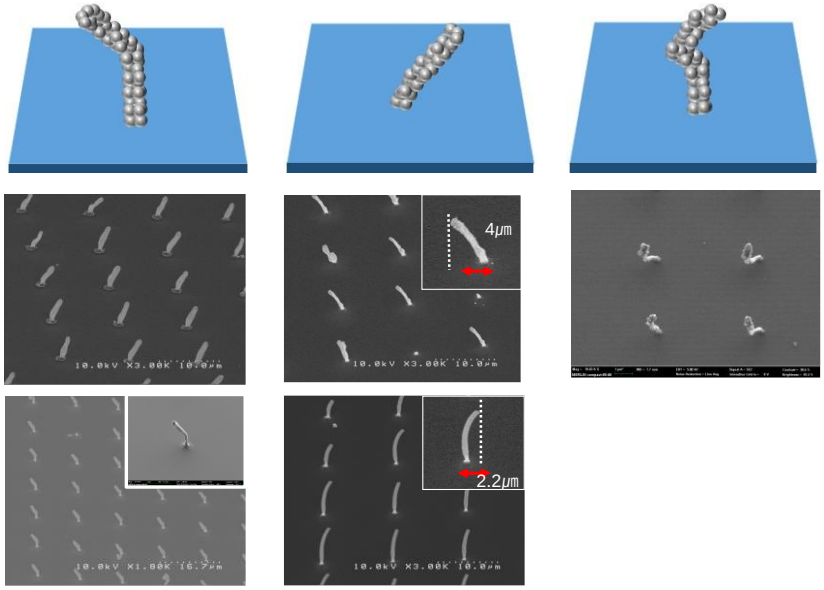

Figure 5.10. Various nanoparticle structure fabricated by 3D printing

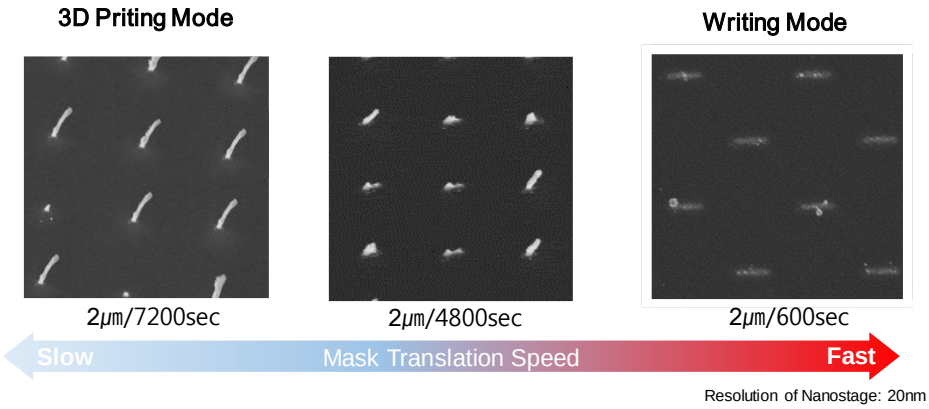

Figure 5.11 Difference of the shape of the nanoparticle structure depending on the translation speed

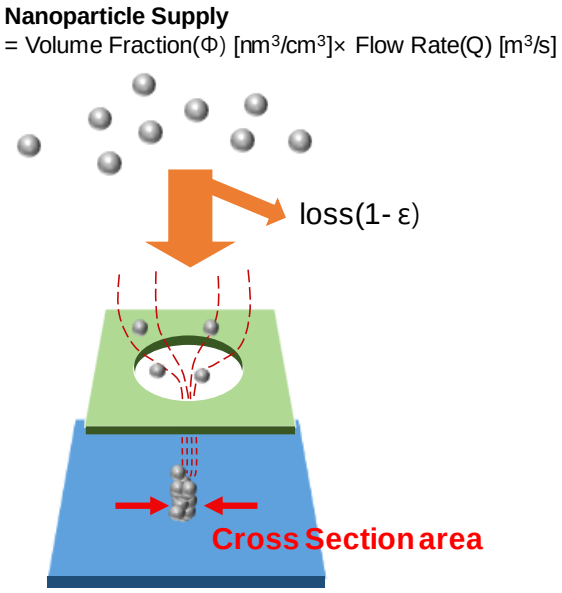

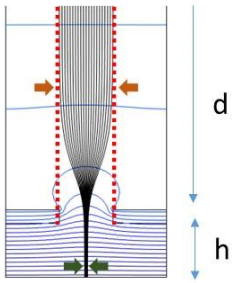

$$E_{avg.upper} = \frac{V_{mask}}{d}$$

$$E_{avg.lower} = \frac{V_{sub} - V_{mask}}{h} = \frac{\Delta V}{h}$$

Density of electric field line ∝ Electric field intensity

$$\text{Focusing ratio} = \frac{\text{Electric field upper side of the mask}}{\text{Electric field lower side of the mask}} = \frac{h \cdot V_{mask}}{d \cdot \nabla V}$$

Figure 5.12 Calculation of the vertical growth rate of the nanoparticle structure

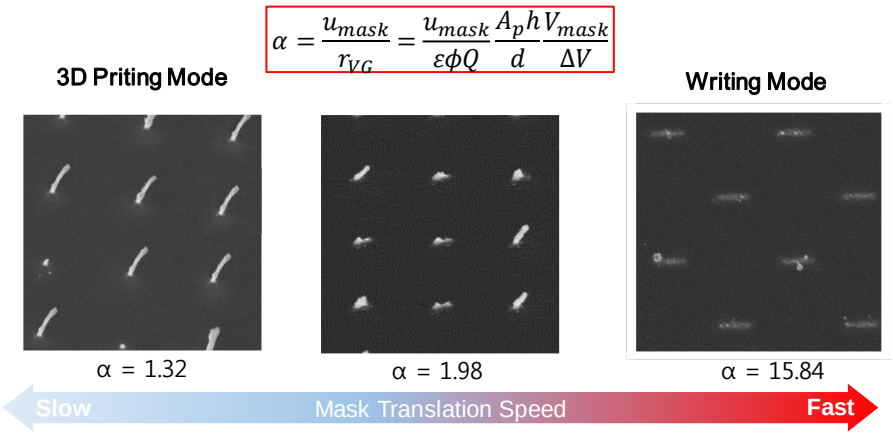

Figure 5.13 Modified mask translation speed

5.5. Conclusion

We have fabricate 3D nanoparticle structure by translating the mask in deposition process. Depending on the translation speed, nanoparticle deposition process was divided into 2 different modes; writing mode and 3D printing mode. In high speed translation, nanoparticle cluster could not be growing to induce the antenna effect, so in-coming nanoparticles were deposited aside of the nanoparticle cluster. In low speed translation, nanoparticle cluster could be growing to induce antenna effect, nanoparticles were deposited onto the existing nanoparticle cluster. By controlling the translation shape and speed, various shapes of nanoparticle structure were fabricated. We proposed new parameters called modified translation speed which could be used as the criteria for separating the 3D printing mode and writing mode.

6. Concluding Remarks

We demonstrated a general methodology for 3D nanoparticle assembly producing various 3D nanoparticle structure in a parallel, inexpensive, and flexible way with nanoscale resolution.

In chapter 2, we studied factors affecting the electrostatic lens effect. 3 factors – ion accumulation voltage, deposition voltage, and mask-substrate distance – were closely examined and the experiment result was validated by nanoparticle trajectory simulation. In studying the effect of the deposition voltage, the discrepancy between the experiment and the simulation result was found and we figured out Brownian diffusion acted great effect on the nanoparticle motion in the low deposition voltage region.

By changing deposition voltage during the deposition process, the core-shell shape nanoparticle structure was fabricated and the mechanism of core-shell fabrication was examined.

In chapter 3, we demonstrate controlled printing of charged nanoparticles using a metal coated stencil mask by applying an electric potential to engineer the electric field streamlines through the mask opening. The potential difference between the metal coated mask and the substrate generates an electrostatic lens effect which focuses the charged nanoparticles toward the center of the opening and hence reduces the size of the printed nanoparticle clusters. In contrast to previously reported ion induced focusing approach, the present method does not rely on ion accumulation, but simply requires changing the potential difference between the mask and the substrate to control the focusing of charged aerosols. By adjusting the potential difference between the mask and the substrate, electric field distortion near the mask opening can be precisely controlled. Using this approach, the printed patterns can be scaled down by up

to a factor of 7.3 in each dimension from the mask opening, which enables printing of sub-micrometer sized particle clusters using a mask with micrometer scale opening sizes. Particle trajectories were calculated by solving the Langevin equation, and the resulting particle deposition profile was compared with the experimental results. Using this approach, a multi-material nanoparticle cluster array was fabricated by a sequential deposition of silver and copper nanoparticles after lateral translation of the mask, resulting in offset arrays of silver and copper nanoparticle clusters on the same substrate

In the application part, we have fabricate 3D nanoparticle structure by translating the mask in deposition process. Depending on the translation speed, nanoparticle deposition process was divided into 2 different modes; writing mode and 3D printing mode. In high speed translation, nanoparticle cluster could not be growing to induce the antenna effect, so in-coming nanoparticles were deposited aside of the nanoparticle cluster. In low speed translation, nanoparticle cluster could be growing to induce antenna effect, nanoparticles were deposited onto the existing nanoparticle cluster. By controlling the translation shape and speed, various shape of nanoparticle structure was fabricated.

References

Bullen, D., S. W. Wang X. Chung, J. Zou, C. A. Mirkin and C. Liu. "Parallel Dip-Pen Nanolithography with Arrays of Individually Addressable Cantilevers." *Appl. Phys. Lett.* 84, (2004): 789-791.

Chae, S., D. Lee, M. C. Kim, D. S. Kim and M. Choi. "A Study of a Wire-in-Hole Type Spark Discharge Generator for Consistent Generation of Unagglomerated Nanoparticles." *Proceedings of the 2014 international aerosol conference.*, (2014).

Chen, D. R. "Design and Evaluation of a Nanometer Aerosol Differential Mobility Analyzer (Nano-Dma)." *J. Aerosol Sci.* 29, (1998): 497-509.

Cheng, W., N. Park, M. T. Walter, M. R. Hartman and D. Luo. "Nanopatterning Self-Assembled Nanoparticle Superlattices by Moulding Microdroplets." *Nature Nanotechnology* 3, no. 11 (2008): 682-690.

Cheng, Wenlong, Nokyoung Park, M. Todd Walter, Mark R. Hartman and Dan Luo. "Nanopatterning Self-Assembled Nanoparticle Superlattices by Moulding Microdroplets." *Nat Nano* 3, no. 11 (2008): 682-690.

Choi, Hoseop, Seunghyon Kang, Wooik Jung, Yoon-ho Jung, Sei Jin Park, Dae Seong Kim and Mansoo Choi. "Controlled Electrostatic Focusing of Charged Aerosol Nanoparticles Via an Electrified Mask." *Journal of Aerosol Science* 88, (2015): 90-97.

Chou, S. Y., P. R. Krauss and P. J. Renstrom. "Imprint Lithography with 25-Nanometer Resolution." *Science* 272, (1996): 85-87.

Demirörs, A. F., P. P. Pillai, B. Kowalczyk and B. A. Grzybowski. "Colloidal Assembly Directed by Virtual Magnetic Moulds." *Nature* 503, no. 7474 (2013): 99-103.

DiFonzo, F. "Focused Nanoparticle-Beam Deposition of Patterned Microstructures." *Appl. Phy. Lett.* 77, (2000): 910-912.

Ergin, T., N. Stenger, P. Brenner, J. B. Pendry and M. Wegener. "Three-Dimensional Invisibility Cloak at Optical Wavelengths." *Science* 328, no. 5976 (2010): 337-339.

Fudouzi, H., M. Kobayashi and N. Shinya. "Site-Controlled Deposition of Microsized Particles Using an Electrostatic Assembly." *Adv. Mater.* 14, (2002): 1649-1652.

Guo, C. X., M. Wang, T. Chen, X. W. Lou and C. M. Li. "A Hierarchically Nanostructured Composite of Mno 2/Conjugated Polymer/Graphene for High-Performance Lithium Ion Batteries." *Advanced Energy Materials* 1, no. 5 (2011): 736-741.

Ha, K., H. Choi, K. Jung, K. Han, J. K. Lee and K. Ahn. "Large-Area Assembly of Three-Dimensional Nanoparticle Structures Via Ion Assisted Aerosol Lithography with a Multi-Pin Spark Discharge Generator." *Nanotechnology* 25, (2014): 225302.

Hamann, H. F., S. I. Woods and S. Sun. "Direct Thermal Patterning of Self-Assembled Nanoparticles." *Nano Lett.* 3, (2003): 1643-1645.

Han, K., W. Kim, J. Yu, J. Lee, H. Lee, C. Gyu Woo and M. Choi. "A Study of Pin-to-Plate Type Spark Discharge Generator for Producing Unagglomerated Nanoaerosols." *Journal of Aerosol Science* 52, (2012): 80-88.

Hayward, R. C., D. A. Saville and I. A. Aksay. "Electrophoretic Assembly of Colloidal Crystals with Optically Tunable Micropatterns." *Nature* 404, (2000): 56-59.

Hinds, W. C. "Aerosol Technology: Properties, Behavior, and Measurement of Airborne Particles." 323-338, 1999.

Jacobs, H. O., S. A. Campbell and M. G. Steward. "Approaching Nanoxerography: The Use of Electrostatic Forces to Position Nanoparticles with 100 Nm Scale Resolution." *Adv. Mater.* 14,

(2002): 1553-1557.

Jacobs, H. O. and G. M. Whitesides. "Submicrometer Patterning of Charge in Thin-Film Electrets." *Science* 291, (2001): 1763-1766.

Jayasinghe, S. N., M. J. Edirisinghe and D. Z. Wang. "Controlled Deposition of Nanoparticle Clusters by Electrohydrodynamic Atomization." *Nanotechnology* 15, (2004): 1519-1523.

Jiang, L., W. Wang, H. Fuchs and L. Chi. "One-Dimensional Arrangement of Gold Nanoparticles with Tunable Interparticle Distance." *Small* 5, no. 24 (2009): 2819-2822.

Kalsin, A. M., M. Fialkowski, M. Paszewski, S. K. Smoukov, K. J. M. Bishop and B. A. Grzybowski. "Electrostatic Self-Assembly of Binary Nanoparticle Crystals with a Diamond-Like Lattice." *Science* 312, no. 5772 (2006): 420-424.

Kang, M. "Nanoparticle Pattern Deposition from Gas Phase onto Charged Flat Surface." *Microelectron. Eng* 71, (2004): 229-236.

Kim, D., P. V. Pikhitsa, H. Yang and M. Choi. "Room Temperature Co and H2 Sensing with Carbon Nanoparticles." *Nanotechnology* 22, no. 48 (2011).

Kim, H., J. Kim, H. Yang, J. Suh, T. Kim, B. Han, S. Kim, D. S. Kim, P. V. Pikhitsa and M. Choi. "Parallel Patterning of Nanoparticles Via Electrodynamic Focusing of Charged Aerosols." *Nature nanotechnology* 1, no. 2 (2006): 117-121.

Klimov, V. I. "Optical Gain and Stimulated Emission in Nanocrystal Quantum Dots." *Science* 290, (2000): 314-317.

Kraus, T., L. Malaquin, H. Schmid, W. Riess, N. D. Spencer and H. Wolf. "Nanoparticle Printing with Single-Particle Resolution." *Nature Nanotechnology* 2, no. 9 (2007): 570-576.

Krinke, T. J. "Positioning of Nanometer-Sized Particles on Flat Surfaces by Direct Deposition from the Gas Phase." *Appl. Phys. Lett.* 78, (2001): 3708-3710.

Krinke, T. J., K. Deppert, M. H. Magnusson and H. Fissan. "Nanostructured Deposition of Nanoparticles from the Gas Phase." *Part. Part. Syst. Charact.* 19, (2002): 321-326.

Krinke, T. J., H. Fissan, K. Deppert, M. H. Magnusson and L. Samuelson. "Positioning of Nanometer-Sized Particles on Flat Surfaces by Direct Deposition from the Gas Phase." *Applied Physics Letters* 78, no. 23 (2001): 3708-3710.

Kruis, F. E., H. Fissan and A. Peled. "Synthesis of Nanoparticles in the Gas Phase for Electronic, Optical and Magnetic Applications[Mdash]a Review." *J. Aerosol Sci.* 29, (1998): 511-535.

Lee, D., S. Yang and M. Choi. "Controlled Formation of Nanoparticles Utilizing Laser Irradiation in a Flame and Their Characteristics." *Appl. Phys. Lett.* 79, (2001): 2459-2461.

Lee, H., S. You, P. V. Pikhitsa, J. Kim, S. Kwon, C. G. Woo and M. Choi. "Three-Dimensional Assembly of Nanoparticles from Charged Aerosols." *Nano Letters* 11, no. 1 (2011): 119-124.

Lee, H., S. You, C. G. Woo, K. Lim, K. Jun and M. Choi. "Focused Patterning of Nanoparticles by Controlling Electric Field Induced Particle Motion." *Applied Physics Letters* 94, no. 5 (2009).

Li, A. and G. Ahmadi. "Dispersion and Deposition of Spherical Particles from Point Sources in a Turbulent Channel Flow." *Aerosol Science and Technology* 16, no. 4 (1992): 209-226.

Lin, Y. "Self-Directed Self-Assembly of Nanoparticle//Copolymer Mixtures." *Nature* 434, (2005): 55-59.

Lin, Y., H. Skaff, T. Emrick, A. D. Dinsmore and T. P. Russell. "Nanoparticle Assembly and Transport at Liquid-Liquid Interfaces." *Science* 299, no. 5604 (2003): 226-229.

Lin, Y., H. Skaff, T. Emrick, A. D. Dinsmore and T. P. Russell. "Nanoparticle Assembly and Transport at Liquid-Liquid Interfaces." *Science* 299, (2003): 226-229.

Liu, P., P. J. Ziemann, D. B. Kittelson and P. H. McMurry. "Generating Particle Beams of Controlled Dimensions and Divergence: I. Theory of Particle Motion in Aerodynamic Lenses and Nozzle Expansions." *Aerosol Sci. Technol.* 22, (1995): 293-313.

Madler, L., H. K. Kammler, R. Mueller and S. E. Pratsinis. "Controlled Systhesis of Nanostructured Particles by Flame Spray Pyrolysis." *J. Aerosol Sci.* 33, (2002): 369-389.

Marina, Y. T., G. Kestutis, G. N. Albert, H. Ville, F. Sami and E. Vladimir. "Lithography-Free Fabrication of Carbon Nanotube Network Transistors." *Nanotechnology* 22, no. 6 (2011): 065303.

Motl, N. E., A. K. P. Mann and S. E. Skrabalak. "Aerosol-Assisted Synthesis and Assembly of Nanoscale Building Blocks." *Journal of Materials Chemistry A* 1, no. 17 (2013): 5193-5202.

Nykypanchuk, D., M. M. Maye, D. Van Der Lelie and O. Gang. "DNA-Guided Crystallization of Colloidal Nanoparticles." *Nature* 451, no. 7178 (2008): 549-552.

Otten, F. "Lithographic Tools for Producing Patterned Films Composed of Gas Phase Generated Nanocrystals." *Mater. Sci. Technol.* 18, (2002): 717-720.

Park, M. H., K. Kim, J. Kim and J. Cho. "Flexible Dimensional Control of High-Capacity Li-Ion-Battery Anodes: From 0d Hollow to 3d Porous Germanium Nanoparticle Assemblies." *Advanced Materials* 22, no. 3 (2010): 415-418.

Peng, X. "Shape Control of Cdse Nanocrystals." *Nature* 404, (2000): 59-61.

Peng, X., L. Manna, W. Yang, J. Wickham, E. Scher, A. Kadavanich and A. P. Alivisatos. "Shape Control of Cdse Nanocrystals." *Nature* 404, no. 6773 (2000): 59-61.

Piseri, P., H. V. Tafreshi and P. Milani. "Manipulation of Nanoparticles in Supersonic Beams for the Production of Nanostructured Materials." *Curr. Opin. Solid State Mater. Sci.* 8, (2004): 195-202.

Ponzoni, A., E. Comini, G. Sberveglieri, J. Zhou, S. Z. Deng, N. S. Xu, Y. Ding and Z. L. Wang. "Ultrasensitive and Highly Selective Gas Sensors Using Three-Dimensional Tungsten Oxide Nanowire Networks." *Applied Physics Letters* 88, no. 20 (2006).

Prost, W. "Monodisperse Aerosol Particle Deposition: Prospects for Nanoelectronics." *Microelectron. Eng.* 41-42, (1998): 535-538.

Prost, W., F. E. Kruis, F. Otten, K. Nielsch, B. Rellinghaus, U. Auer, A. Peled, E. F. Wassermann, H. Fissan and F. J. Tegude. "Monodisperse Aerosol Particle Deposition: Prospects for Nanoelectronics." *Microelectronic Engineering* 41-42, (1998): 535-538.

Ristenpart, W. D., I. A. Aksay and D. A. Saville. "Electrically Guided Assembly of Planar Superlattices in Binary Colloidal Suspensions." *Phys. Rev. Lett.* 90, (2003): 128303.

Salim, A., C. Son and B. Ziaie. "Selective Nanofiber Deposition Via Electrodynamic Focusing." *Nanotechnology* 19, no. 37 (2008).

Suh, J., B. Han, K. Okuyama and M. Choi. "Highly Charging of Nanoparticles through Electrospray of Nanoparticle Suspension." *J. Colloid Interface Sci.* 287, (2005): 135-140.

Tabrizi, N. S., M. Ullmann, V. A. Vons, U. Lafont and A. Schmidt-Ott. "Generation of Nanoparticles by Spark Discharge." *Journal of*

Nanoparticle Research 11, no. 2 (2009): 315-332.

Tao, A. "Langmuir-Blodgett Silver Nanowire Monolayers for Molecular Sensing Using Surface-Enhanced Raman Spectroscopy." *Nano Lett.* 3, (2003): 1229-1233.

van der Eijk, W., W. Oldenof and W. Zehner. "Preparatio of Thin Sources, a Review." *Nuclear Instruments and Methods* 112, no. 1-2 (1973): 343-351.

Visser, J. "On Hamaker Constants: A Comparison between Hamaker Constants and Lifshitz-Van Der Waals Constants." *Advances in Colloid and Interface Science* 3, no. 4 (1972): 331-363.

Von Freymann, G., A. Ledermann, M. Thiel, I. Staude, S. Essig, K. Busch and M. Wegener. "Three-Dimensional Nanostructures for Photonics." *Advanced Functional Materials* 20, no. 7 (2010): 1038-1052.

Vyawahare, S., K. M. Craig and A. Scherer. "Patterning Lines by Capillary Flows." *Nano Letters* 6, no. 2 (2006): 271-276.

Warner, M. G. and J. E. Hutchison. "Linear Assemblies of Nanoparticles Electrostatically Organized on DNA Scaffolds." *Nature Materials* 2, no. 4 (2003): 272-277.

Wolf, H. and R. Birringer. "Pattern Formation in an Array of Magnetic Nanoscale Rods Mimics Magnetic-Dipole Interaction-Driven Spinodal Decomposition." *J. Appl. Phys.* 98, (2004): 074303.

Wolf, H. and R. Birringer. "Pattern Formation in an Array of Magnetic Nanoscale Rods Mimics Magnetic-Dipole Interaction-Driven Spinodal Decomposition." *Journal of Applied Physics* 98, no. 7 (2005).

Woo, C. G., H. Shin, C. Jeong, K. Jun, J. Lee, J. R. Lee, H. Lee, S. You, Y. Son and M. Choi. "Selective Nanopatterning of Protein Via Ion-Induced Focusing and Its Application to Metal-Enhanced Fluorescence." *Small* 7, no. 13 (2011): 1790-1794.

You, S. and M. Choi. "Numerical Simulation of Microscopic Motion and Deposition of Nanoparticles Via Electrodynamic Focusing." *Journal of Aerosol Science* 38, no. 11 (2007): 1140-1149.

You, S., K. Han, H. Kim, H. Lee, C. G. Woo, C. Jeong, W. Nam and M. Choi. "High-Resolution, Parallel Patterning of Nanoparticles Via an Ion-Induced Focusing Mask." *Small* 6, no. 19 (2010): 2146-2152.

You, S., H. Kim and M. Choi. "Method for Focusing Patterning Charged Particles Using a Mask with Patterned Holes and the Electrodynamic Focusing Mask Used Therein." (2008).

Zhang, Y., N. K. Grady, C. Ayala-Orozco and N. J. Halas. "Three-Dimensional Nanostructures as Highly Efficient Generators of Second Harmonic Light." *Nano Letters* 11, no. 12 (2011): 5519-5523.

국문초록

전기장 보조 에어로졸 리소그래피를 이용한 3 차원 나노입자 조립

서울대학교 대학원 기계항공공학부

최 호 섭

나노입자는 기존의 물질이 지니는 특성에 비해 우수한 물리적, 화학적 특성으로 인하여 나노기술의 핵심적인 구성 요소로 연구되고 있다. 원하는 특성을 지닌 기능성 나노입자의 제작기술은 전세계적으로 많은 관심을 받고 있으며, 우수한 성과들이 발표되고 있지만 이러한 나노 입자를 실제 연구 혹은 산업현장에서 사용하기 위해서는 이를 원하는 형상으로 조립하거나 원하는 위치에 배열하는 나노 입자 조립 기술이 필수적이다. 본 연구실에서는 정전기적 집속 방식에 의한 나노 입자 조립기술 (Ion Assisted Aerosol Lithography)을 발표하였으며, 본 기술은 하전된 나노 입자를 전기장의 조절을 통하여 원하는 위치에 배열하거나 혹은 3 차원 형상으로 조립하는 기술이다. 본 연구는 기존의 IAAL 을

발전시켜 능동적으로 원하는 형상의 3 차원 나노구조체를 형성하는 기술의 개발에 있다. 이를 위하여 먼저 IAAL 에 영향을 미치는 요인에 대해 연구 하였으며, 이러한 연구를 바탕으로 3 차원 나노 입자 조립기술을 수행하였다. IAAL 에 영향을 미치는 요인으로 이온 증착 전압, 나노입자 증착 전압, 마스크-기판 사이의 거리임을 확인하였으며 다양한 실험조건에서 정전기적 집속 효과의 정도를 관찰하였다. 이온 증착 전압이 증가할수록 마스크 위에 축적되는 이온의 양이 증가 하기 때문에 정전기적 집속 효과가 강해지게 되며, 이로 인하여 패턴의 폭이 감소하게 되는 것을 확인하였다. 나노 입자 증착 전압에 따른 패턴폭의 변화 실험을 통하여 증착 전압에 따른 나노 입자 패턴 폭이 낮은 증착 전압 영역에서 전기장 시뮬레이션과 다름을 확인하였으며, 이와 같은 차이의 원인이 브라우니안 확산임을 밝혀내었다. 이와 같은 요인분석을 바탕으로 다양한 3 차원 나노 입자 구조체를 형성하였으며, 나노 와이어, 다중 물질로 구성된 3 차원 구조체, 코어-쉘 형상의 나노 입자 구조체를 제작하였다.

정전기적 집속 효과의 정밀한 조절을 위하여 마스크에 직접 전압을 가하는 기술을 발전시켰다. 마스크와 기판 사이의 전압 차이로 인하여 마스크 주변의 전기장의 형상이 변화하여 정전기적 집속 렌즈를 형성하게 되며, 이 정전기적 집속 렌즈는 마스크-기판 사이의 전압 차이로 조절 할 수 있음을 시뮬레이션과 실험을 통하여 확인하였다. 이를 통하여 나노 입자 패턴의 폭이 마스크의

크기에 비해 7 배 이상 감소함을 확인하였으며, 마스크의 이동을 통하여 다양한 물질을 원하는 위치에 배열할 수 있음을 보였다.
마지막으로 마스크의 이동을 통한 능동적 3 차원 나노 입자 조립 기술을 구현하였다. 마스크의 이동속도에 따라서 나노 입자의 조립 현상이 3 차원 조립 혹은 나노 입자 쓰기로 나누어짐을 확인하였으며 마스크의 이동속도와 이동 궤적의 조절을 통하여 다양한 3 차원 나노 입자 구조체를 능동적으로 제작할 수 있음을 확인하였다.

주요어: 나노 입자; 전기장 보조 에어로졸 리소그래피; 정전기적 집속 렌즈; 3 차원 프린팅; 정전 마스크
학 번: 2009-20736